

Precise Asteroseismology of the High-amplitude Delta Scuti Star EH Librae, an AE UMa Analogue in the Hertzsprung Gap

Xiran Xie,¹ Jianning Fu,^{1,2,3*} Gang Meng,¹ Lester Fox Machado,⁴ Raúl Michel,⁴ Huifang Xue,^{5,6} Nian Liu,⁷ Zhongyang Liu,¹ Jie Su^{8,9,10} and Mingfeng Qin¹

¹School of Physics and Astronomy, Beijing Normal University, Beijing 100875, People's Republic of China

²Institute for Frontiers in Astronomy and Astrophysics, Beijing Normal University, Beijing 102206, People's Republic of China

³Xinjiang Astronomical Observatory, Chinese Academy of Sciences, Urumqi 830011, Xinjiang, People's Republic of China

⁴Observatorio Astronómico Nacional, Instituto de Astronomía, Universidad Nacional Autónoma de México, A.P. 106, 22800 Ensenada, México

⁵Department of Physics, Taiyuan Normal University, Jinzhong 030619, People's Republic of China

⁶Institute of Computational and Applied Physics, Taiyuan Normal University, Jinzhong 030619, People's Republic of China

⁷School of Physics and Astronomy, China West Normal University, 637009 Nanchong, People's Republic of China

⁸Yunnan Observatories, Chinese Academy of Sciences, Kunming 650216, People's Republic of China

⁹Key Laboratory for the Structure and Evolution of Celestial Objects, Chinese Academy of Sciences, Kunming 650216, People's Republic of China

¹⁰International Centre of Supernovae, Yunnan Key Laboratory, Kunming 650216, People's Republic of China

Accepted XXX. Received YYY; in original form ZZZ

ABSTRACT

A subclass of intermediate mass variables Delta Scuti stars, known as High-amplitude Delta Scuti (HADS) stars, exhibits pronounced radial pulsations with high amplitudes. The ground-based and space-based observations of the HADS star EH Lib are used to help making asteroseismological analysis of this pulsating star. Following the reduction of the light curves, the frequency analysis reveals the fundamental frequency as $f_0 = 11.3105 \text{ c day}^{-1}$ and two more significant frequencies f_1 and f_2 , in addition to the harmonics of f_0 and a linear combination. The period change rate is determined as $(1/P_0)(dP_0/dt) = (5.4 \pm 0.5) \times 10^{-9} \text{ yr}^{-1}$ derived from an O-C diagram, which is constructed from 342 times of maximum light spanning over 70 years. Using these observational constraints, along with the metallicity reported in the literature, we construct theoretical models using the stellar evolution code MESA and calculate the theoretical frequencies of the eigen modes using the oscillation code GYRE. The appropriate models are selected by matching both f_0 and $(1/P_0)(dP_0/dt)$ within their respective uncertainties. The results indicate that the observed period change of EH Lib can be attributed to stellar evolutionary effects. The stellar parameters of EH Lib are derived as: the mass of $1.715 \pm 0.065 M_\odot$, the luminosity of $\log(L/L_\odot) = 1.38 \pm 0.06$, and the age of $(1.14 \pm 0.13) \times 10^9$ years. EH Lib is classified as a single-mode HADS star, locating currently in the Hertzsprung gap, with a helium core and a hydrogen-burning shell. This work expands the asteroseismological sample of HADS stars and establishes a foundation for future investigations into their commonalities and specific properties, thereby advancing our understanding of these variables.

Key words: stars: individual: EH Lib – stars: oscillations – stars: variables: Scuti

1 INTRODUCTION

Asteroseismology, which emerged nearly three decades ago, has grown to a mature field of the modern astrophysics. It offers a unique opportunity to probe the interiors of pulsating stars, bringing new insights in stellar structure and evolution theories (Aerts 2021; Kurtz 2022). As a classical type of variables, Delta Scuti stars are intrinsically pulsating variables of spectral types A to F, with masses roughly ranging from 1.5 to $2.5 M_\odot$. These stars are located at the intersection of the main sequence and the classical instability strip in the Hertzsprung-Russell (HR) diagram and thus considered to be in a stage of central hydrogen or shell hydrogen burning (Breger 1979; Goupil et al. 2005; Aerts et al. 2010). Their oscillations are

driven by the κ mechanism in the second partial ionization zone of helium. Delta Scuti stars typically exhibit radial and/or non-radial p modes, as well as mixed modes. Where low-order p modes have pulsation periods ranging from approximately 18 minutes to 8 hours, and regular spacing sequences of high-order p modes are detected in some Delta Scuti stars (Handler 2009; Uytterhoeven et al. 2011; Holdsworth et al. 2014; Bedding et al. 2020).

High-amplitude Delta Scuti (HADS) stars represent a subclass of Delta Scuti stars, defined by brightness variations in the V-band exceeding 0.1 mag (Templeton et al. 2002), though other sources adopt a threshold of 0.3 mag (Breger 2000). They are rare, as Lee et al. (2008) estimated that less than 1 per cent of Delta Scuti stars are HADS stars. Because the definitions rely solely on light curves phenomenologically, the rarity of HADS stars and the physical distinctions between them and their low-amplitude counterparts remain poorly understood. Nonetheless, HADS stars have similar charac-

* E-mail: jnfu@bnu.edu.cn

teristics to evolved pulsators such as Cepheid variables in the classical instability strip, including asymmetric light curves, period ratios for multi-mode variables, and period–luminosity (P–L) relations (Petersen & Christensen-Dalsgaard 1996; McNamara 2000). Most HADS stars exhibit single or double radial pulsation modes, typically the fundamental and first overtone modes (Fu et al. 2009; Xue et al. 2018; Daszyńska-Daszkiewicz et al. 2022). However, some HADS stars display three or more radial pulsation modes or, in some cases, even non-radial modes (Xue & Niu 2020; Netzel et al. 2022; Niu & Xue 2024). HADS stars generally have low rotational velocities (Rodríguez & Breger 2001), though exceptions exist, such as V2367 Cyg, which has an unusually high rotational velocity of approximately 100 km s⁻¹ (Balona et al. 2012).

The linear period change rates, expressed as $(1/P)(dP/dt)$, derived from long-term observations, are indicators for determining their evolutionary stages (Fu et al. 2008; Yang et al. 2012). For Delta Scuti stars, Breger & Pamyatnykh (1998) predicted that increases of $(1/P)(dP/dt)$ are from 10^{-10} yr⁻¹ on the main sequence to 10^{-7} yr⁻¹ for more evolved variables. Indeed, asteroseismological analyses have placed several HADS stars in the Hertzsprung gap, such as AE UMa and KIC 6382916 (Niu et al. 2017; Niu & Xue 2022). The Hertzsprung gap, located between the main sequence and the red giant branch on the HR diagram, corresponds to one of the most rapid phases of stellar evolution. Studying stars in this region is therefore crucial for improving evolutionary models, and precise asteroseismology of these HADS stars offers an important window (Kippenhahn et al. 2013).

EH Librae ($\alpha_{J2000} = 14^{\text{h}}58^{\text{m}}56^{\text{s}}$, $\delta_{J2000} = -00^{\circ}56'53''$) was first identified as a variable star by A. N. Vyssotsky, who detected variations in its density using an objective prism plate, as indicated by Code (1950). Subsequently, Code (1950) took photoelectric photometry observations, determining a preliminary period of 0.08842 days. Mahdy & Szeidl (1980) suggested that the star exhibits a relatively stable pulsation period, while Jiang & Yang (1981) proposed a signal of binary motion and a possible period change. Joner (1986) observed the star in $uvby - \beta$ filters, estimating a mean effective temperature of $\langle T_{\text{eff}} \rangle = 7840$ K, and a mean surface gravity of $\langle \log g \rangle = 4.08$ dex. Through a spectroscopic survey, Solano & Fernley (1997) derived an effective temperature of $T_{\text{eff}} = 7711$ K using the calibration method proposed by Balona (1994), along with a projected rotational velocity of $v \sin i = 13.30$ km s⁻¹. With high-resolution spectroscopy, Kahraman Aliçavuş et al. (2017) determined the effective temperature of $T_{\text{eff}} = 7300 \pm 100$ K, the surface gravity of $\log g = 3.9 \pm 0.1$ dex, the projected rotational velocity of $v \sin i = 15 \pm 1$ km s⁻¹, and the iron abundance of $\log \epsilon(\text{Fe}) = 7.11 \pm 0.45$ dex. Furthermore, Pena et al. (2017) monitored the star between 2013 and 2016. By combining these observations with previously compiled times of maximum light, they confirmed the existence of a measurable period change rate.

Alias frequencies arising from almost regular gaps in ground-based observations hinder accurate frequency analysis. However, the continuous, high-precision, and long-duration photometric data from the Transiting Exoplanet Survey Satellite (TESS) mission (Ricker et al. 2014, 2015), which performs a near all-sky survey, allows significant advancement in determining the pulsation of EH Lib. Combined with determination of the linear period change rate, more precise constraints can be imposed on its evolutionary stage. Accordingly, our current study aims to determine the stellar structure and evolutionary stage of EH Lib, and construct its asteroseismological models for the first time.

The structure of the paper is as follows. Section 2 presents new photometric observations and associated data reduction procedures.

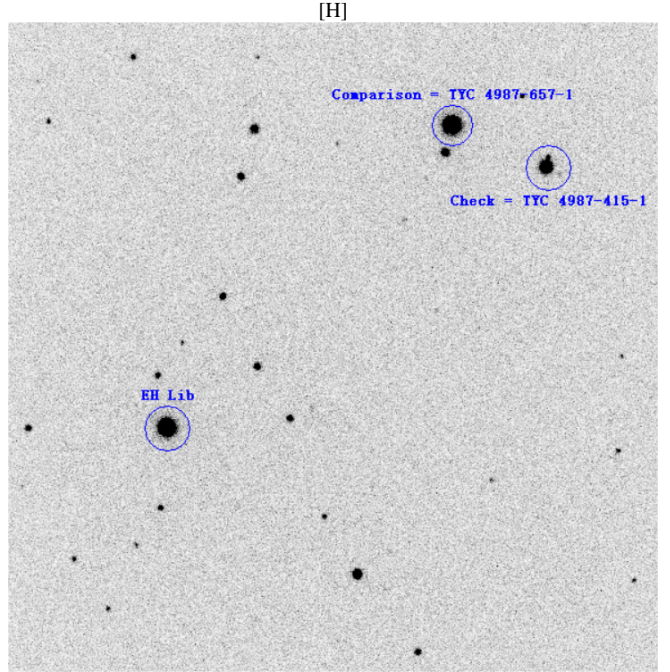


Figure 1. A CCD image of EH Lib taken with the Xinglong 2.16-m Telescope. The field of view is $9'.36 \times 9'.36$. EH Lib, the comparison star (TYC 4987-657-1) and the check star (TYC 4987-415-1) are marked. South is up and East is to the left.

Section 3 focuses on the frequency analysis, mode identification and determination of the period change rate of EH Lib. Section 4 describes the construction of stellar evolutionary tracks and the identification of the optimal models. Section 5 and 6 provide a discussion and conclusions of the study, respectively.

2 OBSERVATIONS AND DATA REDUCTION

In this study, ground-based photometric data collected by our team from 2009 to 2018, along with high-precision space-based observations collected during TESS Sector 51, are utilized.

2.1 Ground-based Photometry

Time-series photometric observations for EH Lib were taken at the Yunnan Astronomical Observatory of China, Xinglong station of National Astronomical Observatories of China, and National Astronomical Observatory San Pedro Martir of Mexico between 2009 and 2018. Figure 1 presents an image of EH Lib taken with the Xinglong 2.16-m Telescope, with EH Lib, the comparison star, and the check star marked. The details of these three stars from SIMBAD¹ (Wenger et al. 2000) are listed in Table 1. A total of 11694 frames were obtained across 55 nights of observations. Table 2 lists the journal of observations.

The observed frames are first corrected by subtracting the master bias and dark frames, and then divided by the master flat frame. Aperture and differential photometry are subsequently performed on EH Lib, the comparison star, and the check star. This procedure is executed using the package IRAF (Tody 1986, 1993) and the software AstroImageJ (Collins et al. 2017). The magnitude differences

¹ <https://simbad.u-strasbg.fr/simbad/>

Table 1. The comparison star and the check star used in the photometry of EH Lib.

Star name	α [J2000]	δ [J2000]	V	B	B - V
Object = EH Librae	14 ^h 58 ^m 55 ^s .92	-00°56'53".01	9.83	10.09	0.26
Comparison = TYC 4987-657-1	14 ^h 58 ^m 39 ^s .80	-01°01'17".63	9.80	10.85	1.05
Check = TYC 4987-415-1	14 ^h 58 ^m 34 ^s .25	-01°00'42".55	11.28	12.52	1.24

Table 2. Journal of the photometric observations for EH Lib. YAO=Yunnan Astronomical Observatory of China, XL=Xinglong station of National Astronomical Observatories of China, SPM=National Astronomical Observatory San Pedro Mártir of Mexico. Telescope=Telescope aperture in cm. Filter symbols: V, R=Johnson V, R.

Date	Observatory	Telescope	CCD	Pixel	Filter	Night	Frames
2009, Feb.	YAO	101.6	Andor DW436	1024×1024	V	10	1254
2014, Feb.	YAO	101.6	Andor DW436	2048×2048	R	6	253
					V	6	254
Mar.	SPM	84	E2V-4240	1076×1024	R	6	805
					V	6	799
	XL	85	PI BFT512	1024×1024	R	6	1415
					V	6	1425
Apr.	XL	85	PI BFT512	1024×1024	R	1	250
					V	1	250
2015, Jan.	YAO	101.6	Andor DW436	1024×1024	R	6	365
					V	9	608
	SPM	84	E2V-4240	1076×1024	V	1	222
Mar.	XL	85	Andor DZ936	2048×2048	R	1	317
					V	1	317
Apr.	SPM	84	E2V-4240	1076×1024	R	4	219
					V	4	215
2016, Feb.	YAO	101.6	Andor DW436	1024×1024	R	4	355
					V	4	358
2017, Jan.	SPM	84	E2V-4240	1036×1024	R	4	288
					V	4	282
2018, Mar.	XL	216	E2V CCD42-40	2048×2048	R	3	1443

between EH Lib and the comparison star are calculated to determine the relative magnitudes of EH Lib. Those between the check star and the comparison star are used to estimate the photometric precisions from the standard deviations of the differential magnitudes.

After data reduction, the whole light curves in V and R bands are presented in Figures A1 and A2, respectively. Figure 2 shows an example of these observed light curves.

2.2 Space-based Photometry

TESS observed EH Lib (TIC 157861023) with a 2-min cadence during Sector 51. All target pixel files (TPFs) are downloaded from the Mikulski Archive for Space Telescopes (MAST)² using the Lightkurve package (Lightkurve Collaboration et al. 2018; Barentsen

et al. 2021). Aperture sizes are carefully selected on the TPFs to produce optimal light curves. After removing outliers and converting the normalized flux to TESS magnitude, a quartic polynomial function is applied to fit and then detrend the light curves, resulting in a total of 10,795 reduced data points. The final TESS light curves are presented in Figure 3.

3 PULSATION ANALYSIS

3.1 Frequency Analysis

Given that the frames observed by TESS provide the most continuous, high-precision, and long-duration data, frequency analysis is performed exclusively on the TESS light curves. The software Period04 (Lenz & Breger 2005) computes discrete Fourier transformations of the light curves to search for significant peaks in the

² <https://archive.stsci.edu>

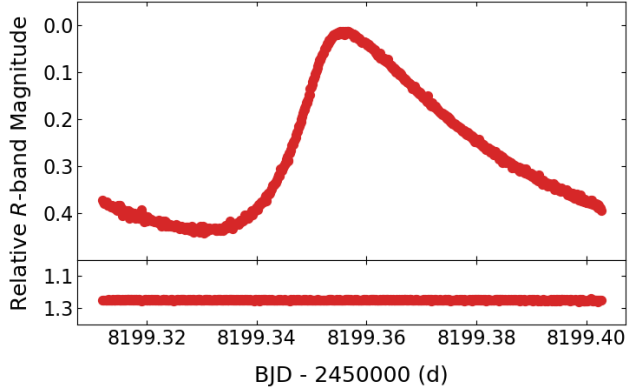


Figure 2. An observed light curve of EH Lib in R -band, taken with the Xinglong 2.16-m Telescope on 21 March 2018. The top panel shows the magnitude differences between EH Lib and the comparison star, and the bottom panel shows the magnitude differences between the check star and the comparison star.

amplitude spectra below Nyquist frequency. In this process, a Hamming window is applied to reduce sidelobes, particularly the first one, thereby enhancing the clarity of the main peaks, and to suppress spectral leakage caused by data gaps and irregular sampling in TESS observations (Harris 1978). The light curves are subsequently fitted based on the extracted frequencies using a least-squares approach with the following formula,

$$m = m_0 + \sum_i A_i \sin(2\pi(f_i t + \phi_i)) \quad (1)$$

Table 3 lists the frequency solution, including the dominant frequency $f_0 = 11.3105 \text{ c day}^{-1}$ and other frequencies, each with a signal-to-noise (S/N) ratio exceeding 5.3 according to the criterion of Baran & Koen (2021). Figure 4 displays the amplitude spectrum with its corresponding spectral window of the TESS light curves, and Figure 3 presents the corresponding fitting curves shown in light blue lines based on the solution. Figure 5 shows the amplitude spectra of the frequency pre-whitening process. Since the low-frequency domain ($0\text{-}2 \text{ c day}^{-1}$) of the amplitude spectra is affected by the systemic noise, such as the spacecraft motions, the instrument sensitivity instability and scattered light contamination, the peaks in this domain are excluded from the analysis.

Candidate linear combinations of the extracted frequencies, expressed as $f_a \pm \sigma_a = f_b \pm \sigma_b \pm f_c \pm \sigma_c$, are evaluated using the criterion of Fu et al. (2013), namely $\sigma_a \leq 3 \times (\sigma_b + \sigma_c)$. When this criterion is satisfied, the component with the lowest amplitude is identified as a combination, while the higher ones as independent frequencies which are f_0 and f_1 for EH Lib. There are no detectable combinations of f_2 . Candidate harmonics of f_0 are identified following the similar criterion.

3.2 Mode Identification

As far as the three frequencies f_0 , f_1 and f_2 of EH Lib listed in Table 3, since the amplitude of f_0 is significantly larger than those of f_1 and f_2 , the corresponding period $P_0 = 0.0884133 \pm 0.0000001$ days of f_0 is the pulsation period P of EH Lib. Based on the typical pulsational characteristics of HADS stars, f_0 is assumed to be a radial mode, while f_1 and f_2 are not. Consequently, once its mode is identified, only $f_0 = 11.310514 \pm 0.000003 \text{ c day}^{-1}$ is used to constrain the stellar models.

Table 3. The frequency solution of the light curves observed by TESS for EH Lib.

No.	ID	Frequency (c day^{-1})	Amplitude (mmag)	S/N
F1	f_0	11.310514(2)	144.01	4351.5
F2	$2f_0$	22.62100(1)	55.96	1937.6
F3	$3f_0$	33.93152(8)	24.01	948.8
F4	$4f_0$	45.24213(0)	12.23	497.2
F5	$5f_0$	56.5525(9)	6.19	294.1
F6	$6f_0$	67.8630(1)	3.73	175.4
F7	$7f_0$	79.1736(0)	2.40	101.8
F8	$8f_0$	90.4842(3)	1.59	70.1
F9	$9f_0$	101.7949(0)	1.06	46.3
F10	$10f_0$	113.104(5)	0.71	32.2
F11	$11f_0$	124.415(2)	0.44	21.6
F12	f_1	21.107(0)	0.37	13.6
F13	$12f_0$	135.726(7)	0.29	12.6
F14	f_2	10.750(0)	0.24	8.0
F15	$13f_0$	147.041(6)	0.17	7.8
F16	$f_0 + f_1$	32.419(7)	0.14	6.3
F17	$14f_0$	158.348(8)	0.13	6.0

Traditionally, pulsation modes can be identified by calculating pulsation constants (Breger & Bregman 1975). The definition is,

$$Q = P \sqrt{\frac{\bar{\rho}}{\bar{\rho}_\odot}} \quad (2)$$

Where P is in days, $\bar{\rho}$ the mean stellar density, and $\bar{\rho}_\odot$ the mean solar density. Following Breger (1990), Equation (2) can be expressed as,

$$\log Q = \log P + 0.5 \log g + 0.1 M_{\text{bol}} + \log T_{\text{eff}} - 6.456 \quad (3)$$

Here, M_{bol} is the absolute bolometric magnitude. Together with M_{bol} , the bolometric luminosity $\log(L/L_\odot)$ of EH Lib is derived from its parallax parallax, $\varpi = 2.7339 \pm 0.0192$ mas, provided by Gaia DR3 (Gaia Collaboration et al. 2023), using the following equations,

$$M_{\text{bol}} = m_G + BC_G - A_G + 5 \log \varpi + 5 \quad (4)$$

$$- 2.5 \log(L/L_\odot) = M_{\text{bol}} - M_{\text{bol},\odot} \quad (5)$$

The calculations incorporate the mean G-band magnitude $m_G = 9.8853 \pm 0.0058$, the interstellar extinction $A_G = 0.1299$, and the bolometric correction $BC_G = 0.019$, estimated following the methods proposed by Jordi et al. (2010) and Andrae et al. (2018). Adopting the absolute bolometric magnitude of the Sun $M_{\text{bol},\odot} = 4.74$ as defined by IAU (Mamajek et al. 2015), the absolute bolometric magnitude of EH Lib is determined as $M_{\text{bol}} = 1.959 \pm 0.064$, corresponding to a bolometric luminosity of $\log(L/L_\odot) = 1.11 \pm 0.03$.

Substituting $P = 0.0884133 \pm 0.0000001$ days, $M_{\text{bol}} = 1.959 \pm 0.064$, the effective temperature $T_{\text{eff}} = 7300 \pm 100$ K and the surface gravity $\log g = 3.9 \pm 0.1$ dex from Kahraman Aliçavuş et al. (2017) into Equation (3) yields a pulsation constant for EH Lib of $Q = 0.032 \pm 0.001$ days. According to Breger & Bregman (1975), fundamental radial modes of Delta Scuti stars typically have $Q > 0.029$ days, thus f_0 satisfies this criterion.

Besides, the pulsation mode can be identified by comparing the V -band absolute magnitude M_V and period P_0 with the newly calibrated P-L relations for Delta Scuti stars (Ziaali et al. 2019; Jayasinghe et al. 2020; Poro et al. 2021; Barac et al. 2022). For instance, Barac

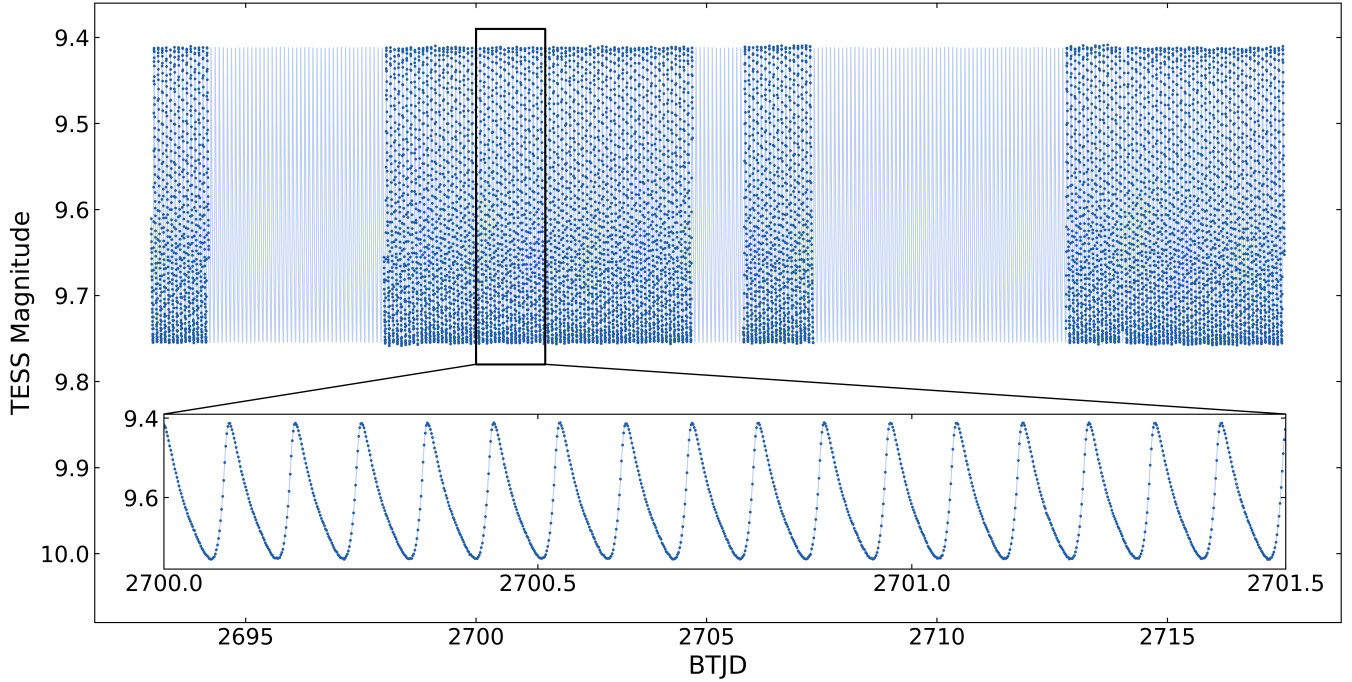


Figure 3. Blue points present all the reduced data points observed by TESS, while the light blue line presents the fitted curve obtained from the extracted frequency solution listed in Table 3. The small panel shows the zoomed-in view of a part of the light curves.

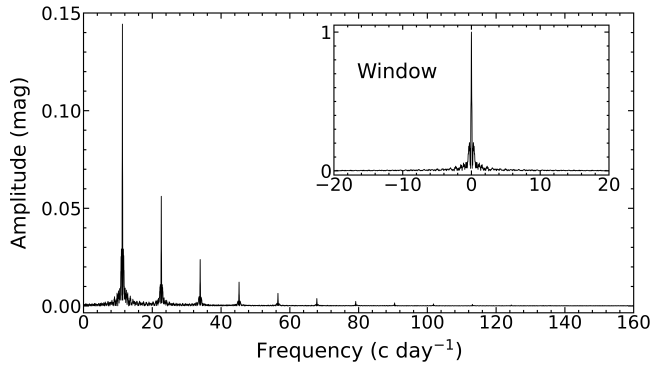


Figure 4. The Fourier amplitude spectrum of the TESS light curves. The corresponding spectral window is shown in the inset.

et al. (2022) derived the following P–L relation for Delta Scuti stars pulsating in the fundamental radial mode,

$$M_V = (-3.01 \pm 0.07) \log(P_0/d) - (1.40 \pm 0.07) \quad (6)$$

Analogously following the methods of Barac et al. (2022), the V-band apparent magnitude $m_V = 9.88$ of EH Lib is obtained from ASAS-SN³, and the corresponding extinction coefficient $A_V = 0.176$ is calculated utilizing the dust-maps Python package of Green et al. (2019). The V-band absolute magnitude M_V is then calculated by the below equation,

$$M_V = m_V + 5 \log \varpi + 5 - A_V \quad (7)$$

Thus, the V-band absolute magnitude of EH Lib is determined as

³ <https://asas-sn.osu.edu/variables>

$M_V = 1.888$. According to Equation (6), a HADS star pulsating in the fundamental radial mode with period P_0 should have $1.627 \leq M_V \leq 1.915$. Moreover, $M_V = 1.888$ is consistent with the corresponding P–L relations of Ziaali et al. (2019); Jayasinghe et al. (2020); Poro et al. (2021).

In one word, f_0 is identified as the fundamental mode of the radial pulsations of EH Lib.

3.3 Period Change Rate

Constraining theoretical models for HADS stars is challenging with only one frequency. Hence, an additional pulsation parameter, period change rate, can be helpful. Typically, the classical O–C method (Sterken 2005) can be used to derive the linear period change rate of single-mode HADS stars. Based on the new observations, light curves around the light maxima of EH Lib are fitted using quartic polynomials to determine the times of maximum light. The uncertainties of these times of maximum light are estimated using the Markov Chain Monte Carlo (MCMC) method with 20,000 iterations performed for each maximum. Typical uncertainties are found to be less than 0.0003 days. Table 4 lists 53 newly determined times of maximum light derived from the ground-based *V*-band observations. The same analysis is applied to the ground-based *R*-band observations and the TESS data, yielding 38 and 158 newly determined times of maximum light, respectively, as listed in Tables A1 and A2.

For the O–C analysis, 93 times of maximum light reported in previous literature (Code 1950; Ashbrook 1952; Fitch 1957; Sanwal & Pande 1961; Fitch et al. 1966; Oosterhoff & Walraven 1966; Kertnikov & Medvedev 1977; Garrido et al. 1979; Mahdy & Szeidl 1980; Jiang & Yang 1981; Hamdy 1985; Joner 1986; Yang et al. 1992; Pena et al. 2017), as listed in Table A3, are combined with the newly determined values. Since the uncertainties for the times of maximum light reported in the literature were not provided, weights are assigned

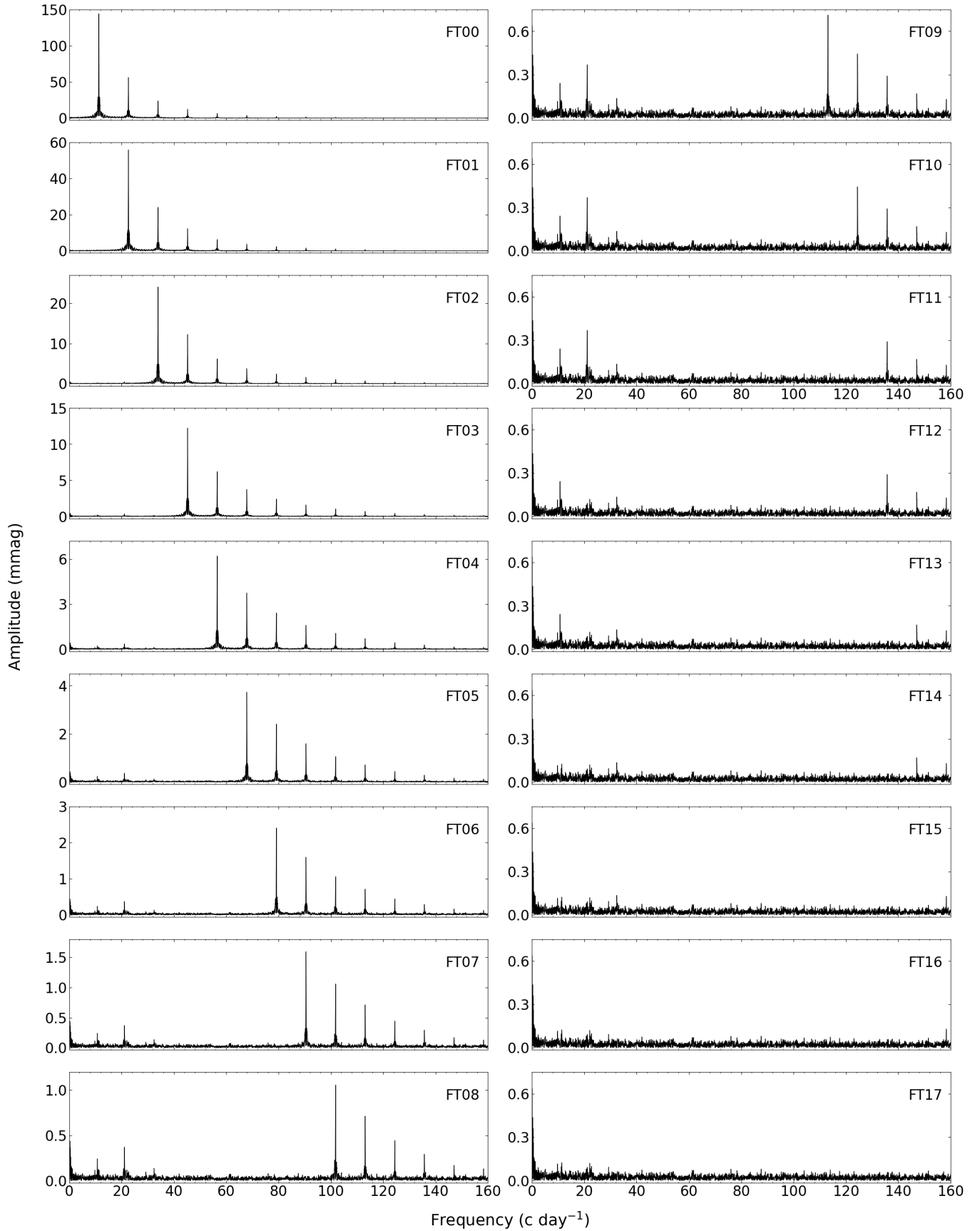


Figure 5. The Fourier amplitude spectra of the TESS light curves with the frequency pre-whitening process shown.

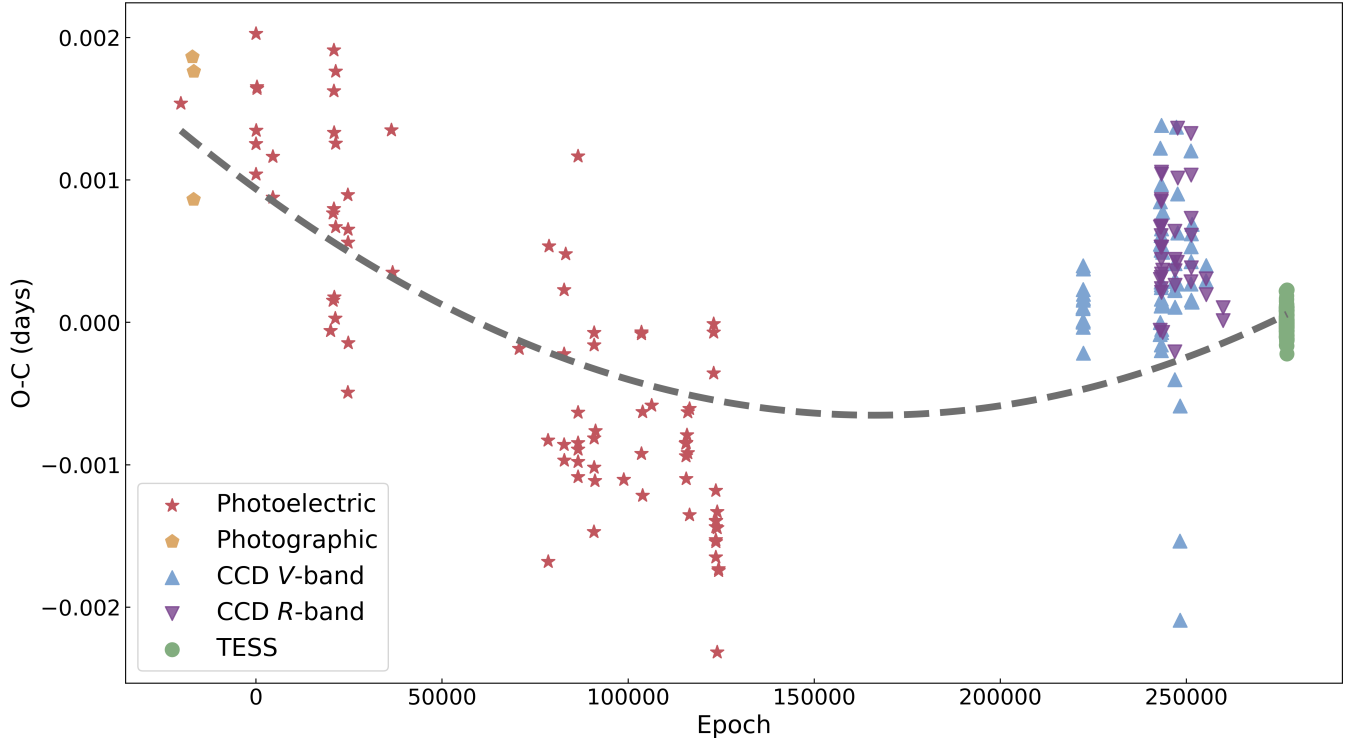


Figure 6. O-C diagram for EH Lib calculated using the ephemeris from Equation (8), with the parabolic polynomial fit represented by a dashed curve. Different markers indicate data obtained from various detector types: red stars for photoelectric, orange pentagons for photographic, blue up-pointing triangles for CCD V-band, purple down-pointing triangles for CCD R-band and green circles for TESS data, as described in the labels.

according to the detector type: 0.5 for photographic, 0.9 for photoelectric, 1.0 for CCD V-band, and 2.0 for TESS data. Additionally, for a given pulsation period, there is a systematic offset between the O-C values derived from *V*-band and *R*-band observations, with a mean difference of 0.00011 days and a standard deviation of 0.00030 days. To account for this discrepancy, a weight of 0.1 is assigned to CCD *R*-band data. Furthermore, to correct for the effects of leap seconds, motion, and related factors, all time stamps used in this study are converted to Barycentric Julian Date (BJD) in Barycentric Dynamical Time (TDB). Incorporating these weights, along with the pulsation period determined from TESS observations, the data are used to derive the linear ephemeris formula,

$$C = \text{BJD } 2435223.7587 + 0.088413267 \times E \quad (8)$$

Figure 6 presents the O-C diagram, which exhibits long-term variability. As a result, a parabolic polynomial is used to fit the times of maximum light, as indicated by the dashed curve. Incorporating the assigned weights, the parabolic term is determined, yielding the following parabolic ephemeris,

$$C = \text{BJD } 2435223.7596 + 0.088413248 \times E + 5.76 \times 10^{-14} E^2 \quad (9)$$

The residuals of the fit yield a root-mean-square (RMS) value of 0.00057 days. The parabolic coefficient deviates from zero by 11.34σ , demonstrating the necessity of the parabolic fit.

Considering that EH Lib is a single-mode HADS star, whose pulsation is dominated by f_0 , the period change rate of f_0 is consistent with that of the star. Based on the parabolic term in Equation (9), the period change rate of f_0 can be derived as follows,

$$\frac{1}{P_0} \frac{dP_0}{dt} = -\frac{1}{f_0} \frac{df_0}{dt} = (5.4 \pm 0.5) \times 10^{-9} \text{ yr}^{-1} \quad (10)$$

4 THEORETICAL MODELING

In this section, the theoretical models of EH Lib are constructed to constrain the stellar parameters of the star, using the open-knowledge software instrument Modules for Experiments in Stellar Astrophysics (MESA; Paxton et al. 2011, 2013, 2015, 2018, 2019; Jermyn et al. 2023). The one-dimensional stellar evolution module, MESA star, is used to compute stellar evolutionary tracks for different initial input parameters. Furthermore, the stellar oscillation code, GYRE (Townsend & Teitler 2013; Townsend et al. 2018; Goldstein & Townsend 2020) coupled with MESA, is used to calculate the frequencies of the eigen modes at each step along the evolutionary tracks.

4.1 Physical Parameters

The high-resolution spectra of EH Lib, obtained by Kahraman Aliçavuş et al. (2017) using the ARC Echelle Spectrograph (ARCES) mounted at the 3.5-m telescope of the Apache Point Observatory (USA), provides the basis for determination of stellar parameters of this star. The spectra cover a wavelength range of 3200–10000 Å with a resolving power of $R \sim 31500$. Based on the reported iron abundance from Kahraman Aliçavuş et al. (2017), the metallicity of EH Lib is estimated as $[\text{Fe}/\text{H}] = -0.39$, which is adopted for subsequent calculations.

Table 4. Times of maximum light of EH Lib from new ground-based V-band observations. T_{\max} is in BJD-2450000, O-C is in days. Epoch and O-C are derived from the ephemeris formula in Equation (8).

T_{\max}	Epoch	O-C	T_{\max}	Epoch	O-C
4867.41847	222180	0.00011	6732.31957	243273	0.00016
4868.39101	222191	0.00010	6733.02737	243281	0.00066
4869.36346	222202	0.00000	6734.97318	243303	0.00138
4872.45792	222237	0.00000	6736.29793	243318	-0.00007
4873.34221	222247	0.00016	6736.38696	243319	0.00055
4873.43086	222248	0.00040	6737.27050	243329	-0.00005
4874.31456	222258	-0.00003	6761.23103	243600	0.00049
4874.40302	222259	0.00001	6761.31973	243601	0.00077
4875.28737	222269	0.00023	7049.45802	246860	0.00022
4877.32085	222292	0.00020	7050.42994	246871	-0.00040
4878.29298	222303	-0.00022	7052.46407	246894	0.00023
4878.38198	222304	0.00038	7053.43668	246905	0.00029
4879.35432	222315	0.00017	7054.40935	246916	0.00041
6703.40818	242946	-0.00008	7056.44274	246939	0.00030
6704.38081	242957	0.00000	7057.41509	246950	0.00011
6705.35458	242968	0.00122	7106.30779	247503	0.00027
6705.44232	242969	0.00055	7117.80215	247633	0.00090
6708.36025	243002	0.00085	7119.83538	247656	0.00063
6723.92026	243178	0.00012	7435.29449	251224	0.00120
6724.00917	243179	0.00061	7435.38197	251225	0.00027
6725.95393	243201	0.00028	7437.32722	251247	0.00043
6726.04257	243202	0.00051	7440.33338	251281	0.00053
6729.31362	243239	0.00026	7441.30601	251292	0.00062
6729.40201	243240	0.00024	7441.39396	251293	0.00016
6730.37411	243251	-0.00020	7795.04716	255293	0.00029
6730.99417	243258	0.00097	7798.93745	255337	0.00040
6731.34670	243262	-0.00016			

The initial metal abundance Z is calculated using the approximation proposed by Bressan et al. (2012), as described in Wang et al. (2021),

$$[\text{Fe}/\text{H}] = \log(Z/X) - \log(Z/X)_\odot \quad (11)$$

$$Y = 0.2485 + 1.78Z \quad (12)$$

$$X + Y + Z = 1 \quad (13)$$

Here, $(Z/X)_\odot = 0.0207$ (Bressan et al. 2012) and Y represents the helium abundance. The metal abundance is estimated as $Z = 0.006$.

4.2 Setup of the Model Calculation

Since EH Lib is classified as a HADS star, stellar evolutionary tracks are constructed for masses ranging from $1.50 M_\odot$ to $2.50 M_\odot$ with the step size of $0.01 M_\odot$. As described previously, the metal abundance Z is determined as 0.006 from the metallicity value $[\text{Fe}/\text{H}] = -0.39$.

The mixing-length parameter α_{MLT} is fixed at 1.89, following Yang et al. (2012), which has an insignificant effect on the models. The convective overshooting parameter is set as $f_{\text{ov}} = 0.015$ following Niu et al. (2017). The rotational effects are neglected in the modeling, given that EH Lib is a slow rotator.

Each evolutionary track commences from the zero-age main sequence and progresses through the post main sequence stages, with the specified initial mass and chemical composition (X, Y, Z). At each evolutionary step, the pulsation frequencies are computed using the oscillation code GYRE.

4.3 Parameter Fitting

To constrain the stellar models, the frequency of the fundamental mode f_0 detected from TESS light curves is used. Additionally, the period change rate $(1/P_0)(dP_0/dt)$ determined in this study falls within the range predicted for Delta Scuti stars by Breger & Pamyatnykh (1998). Therefore, this rate can be attributed to stellar evolutionary effects, making it another valuable criterion for constraining models.

Figure 7 displays the evolutionary tracks from the zero-age main sequence to the end of post main sequence stages, computed with an age step size of 10^5 yr for masses ranging from $1.50 M_\odot$ to $2.50 M_\odot$ with a mass step size of $0.01 M_\odot$. Because the observed frequency uncertainty, which is approximately $3 \times 10^{-6} \text{ c day}^{-1}$, is significantly lower than the calculated uncertainty, which is approximately 0.003 c day^{-1} , the black regions on the tracks present the models for which the calculated frequency of the fundamental mode f_0 matches the observed f_0 within the calculated uncertainty. The blue regions indicate the models for which the calculated period change rate $(1/P_0)(dP_0/dt)$ aligns with the observed $(1/P_0)(dP_0/dt)$ within 1σ uncertainty. The red regions mark the models that satisfy both criteria simultaneously.

The Details of the fitted models are provided in Table 5, and the derived stellar parameters of EH Lib are summarized in Table 6. Figure 8 shows the positions of the fitted models on the HR diagram.

The internal structure and evolutionary stage of EH Lib are investigated using these fitted stellar models. Taking the model with a mass of $1.715 M_\odot$ as an example, Figures 9 and 10 respectively illustrate the internal distributions of elemental abundances and energy generation rates against fractional stellar radius. These figures indicate that EH Lib has exhausted hydrogen in its core, resulting in the formation of a helium core, surrounded by a hydrogen-burning shell where the energy is currently generated. This suggests that the star has evolved off the main sequence and is currently ascending the subgiant branch in the HR diagram.

5 DISCUSSION

Jiang & Yang (1981) obtained 6 new times of maximum light for EH Lib with a high-speed photoelectric photometer. Combining these measurements with earlier photoelectric data, they were the first to propose the hypothesis that EH Lib may reside in a binary system. In contrast, the O-C analysis of this study reveals no clear evidence for orbital motion, although the binarity cannot be entirely ruled out due to the limited time span and observing gaps. Similarly, Kervella et al. (2019) suggested variations in proper motion that hint at a possible companion, but they cautioned that the S/N ratio was too low for a firm conclusion. To settle this issue definitively, further continuous, precise and long-duration observations are required. If EH Lib is actually in a binary system, the independent orbital parameters could provide valuable additional constraints for the theoretical modeling.

Constraining stellar models for a single-mode HADS star like EH Lib meets significant challenges, as discussed in Section 3, due to a large number of models match the observed frequency within the uncertainties, as shown in Figure 7. However, incorporating the period change rate as an additional constraint has proven effective, as demonstrated in Figures 7 and 8. These results also confirm that the observed period change rate of EH Lib can be attributed to the stellar evolutionary effects.

When comparing the theoretical luminosity $\log(L_{\text{theo}}/L_\odot) =$

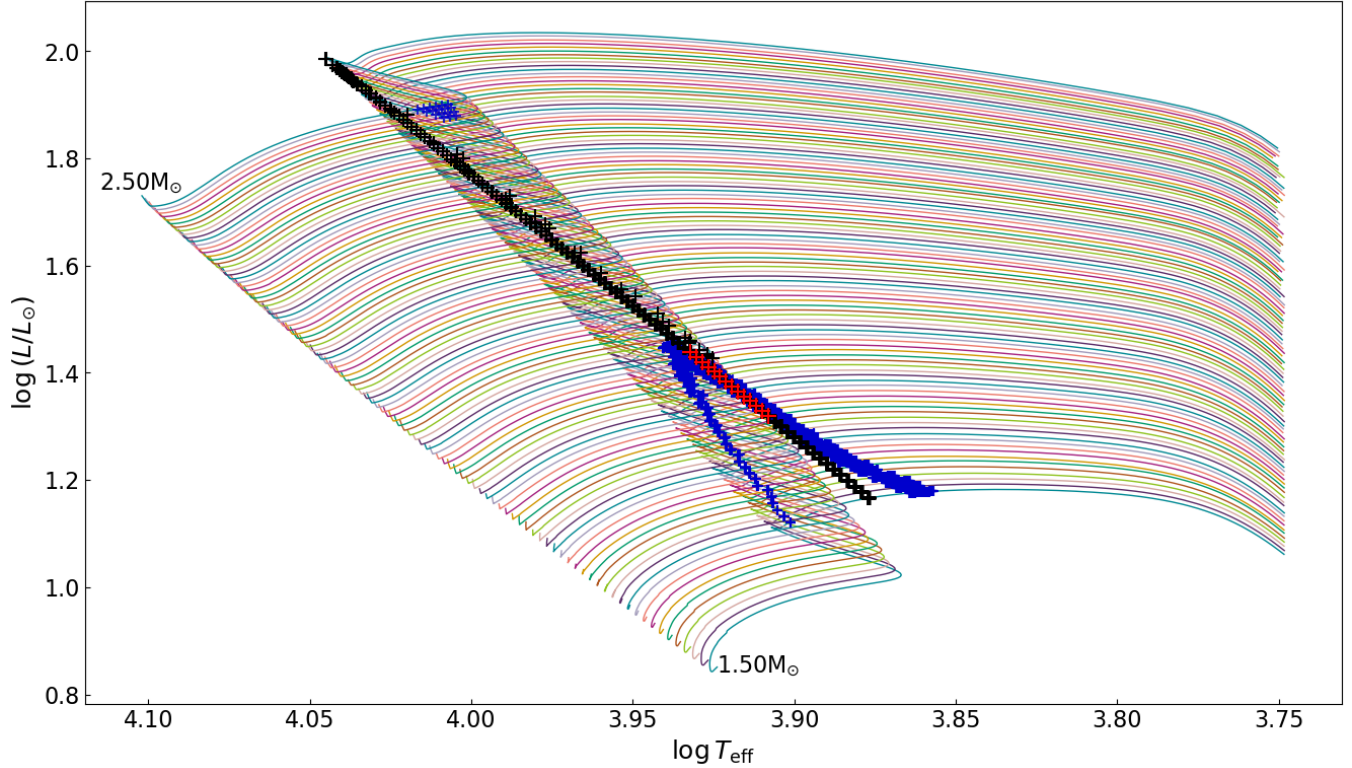


Figure 7. Evolutionary tracks from the zero-age main sequence to the end of post main sequence stages, computed with an age step size of 10^5 yr for masses ranging from $1.50 M_\odot$ to $2.50 M_\odot$, with a mass step size of $0.01 M_\odot$. The black regions on the tracks present the models for which the calculated frequency of the fundamental mode f_0 matches the observed f_0 within the calculated uncertainty. The blue regions indicate the models for which the calculated period change rate $(1/P_0)(dP_0/dt)$ aligns with the observed $(1/P_0)(dP_0/dt)$ within 1σ uncertainty. The red regions mark the models that satisfy both criteria simultaneously.

Table 5. The fitted stellar models for EH Lib.

$M (M_\odot)$	Age (10^9 yr)	T_{eff} (K)	$\log (L/L_\odot)$	$\log g$ (dex)	f_0 (c day $^{-1}$)	$\frac{1}{P_0} \frac{dP_0}{dt}$ ($\times 10^{-9}$ yr $^{-1}$)
1.65	1.273	3.9079	1.3185	3.9234	11.3116	5.00
1.66	1.250	3.9098	1.3278	3.9242	11.3103	4.94
1.67	1.227	3.9118	1.3374	3.9251	11.3119	5.12
1.68	1.209	3.9136	1.3468	3.9258	11.3091	5.11
1.69	1.190	3.9155	1.3559	3.9268	11.3123	5.07
1.70	1.167	3.9174	1.3653	3.9275	11.3100	5.27
1.71	1.150	3.9192	1.3743	3.9283	11.3104	5.20
1.72	1.127	3.9211	1.3836	3.9292	11.3112	5.40
1.73	1.111	3.9230	1.3930	3.9299	11.3090	5.43
1.74	1.091	3.9248	1.4017	3.9307	11.3095	5.45
1.75	1.072	3.9267	1.4107	3.9318	11.3135	5.48
1.76	1.056	3.9285	1.4199	3.9325	11.3127	5.66
1.77	1.038	3.9304	1.4289	3.9334	11.3137	5.80
1.78	1.024	3.9322	1.4378	3.9340	11.3102	5.84

1.38 ± 0.06 from the fitted models listed in Table 5 with the luminosity $\log (L_{\text{Gaia}}/L_\odot) = 1.11 \pm 0.03$ from Gaia observations, it is found that the theoretical one of EH Lib is slightly higher than the observed value. This discrepancy may be due to errors in the determination of the bolometric correction. Additionally, the theoretical effective temperature $T_{\text{eff, theo}} = 8321 \pm 232$ K is higher than the observed value $T_{\text{eff, obs}} = 7300 \pm 100$ K from Kahraman Aliçavuş et al. (2017), while the surface gravity $\log g_{\text{theo}} = 3.929 \pm 0.005$ dex derived from theoretical models is in good agreement with the observed

value $\log g_{\text{obs}} = 3.9 \pm 0.1$ dex. All of these results may suggest a more complex process underlying the stellar structures and pulsation mechanisms of HADS stars.

For the frequencies f_1 and f_2 listed in Table 3, the observed values are $f_{1,\text{obs}} = 21.107 \pm 0.001$ c day $^{-1}$ and $f_{2,\text{obs}} = 10.750 \pm 0.002$ c day $^{-1}$. For f_1 , Table 7 lists the calculated frequencies of the fitted models listed in Table 5 that are closest to $f_{1,\text{obs}}$. The harmonic degree is restricted to $l < 4$ because of partial cancellation (Aerts 2021), and the azimuthal order is set as $m = 0$ since the rotational

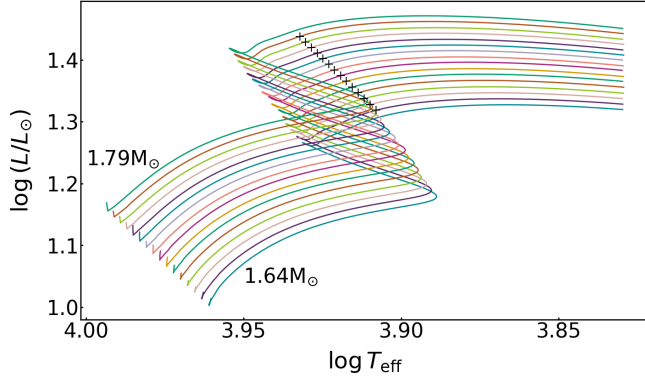


Figure 8. Evolutionary tracks from the zero-age main sequence to the end of post main sequence stages in the mass range of $1.64\text{--}1.79 M_{\odot}$. The black crosses mark the fitted models of EH Lib.

Table 6. The determined stellar parameters of EH Lib.

Parameter	Value
$M (M_{\odot})$	1.715 ± 0.065
Age (10^9 yr)	1.14 ± 0.13
T_{eff} (K)	8321 ± 232
$\log g$ (dex)	3.929 ± 0.005
$\log (L/L_{\odot})$	1.38 ± 0.06

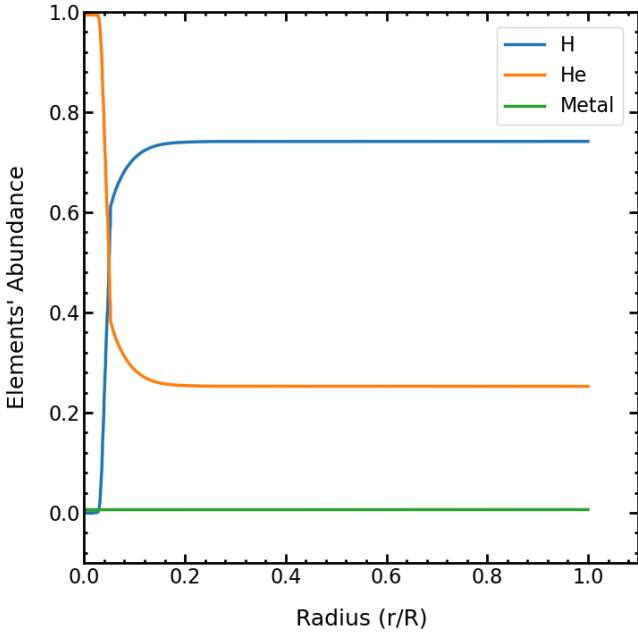


Figure 9. Internal distributions of hydrogen, helium, and metals plotted against fractional stellar radius for the $1.715 M_{\odot}$ model.

effects are neglected. The fact that f_1 corresponds to a mixed mode with the acoustic-wave winding number $n_p = 3$, indicates that EH Lib is an evolved star (Aerts et al. 2010). The frequency f_2 satisfies $f_2 \approx f_1 - f_0 + 1 \text{ c day}^{-1}$. Given its much lower amplitude compared to f_0 , and EH Lib's proximity to the ecliptic, f_2 may be attributed to the combination of f_0 , f_1 and the instrumental effects, such as

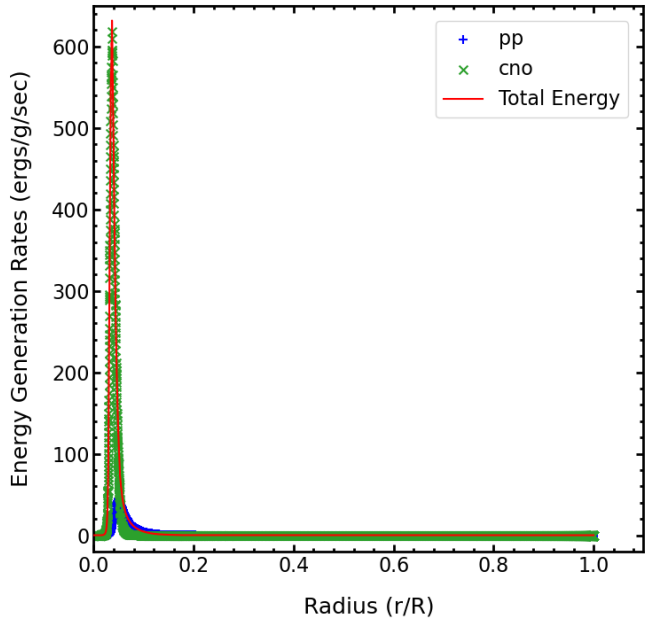


Figure 10. Internal distributions of energy generation rates plotted against fractional stellar radius for the $1.715 M_{\odot}$ model.

Table 7. The calculated $f_{1,\text{cal}}$ of the fitted models listed in Table 5 that are closest to $f_{1,\text{obs}}$. Here, n_p denotes the acoustic-wave winding number, n_g the gravity-wave winding number, and l the harmonic degree. $\Delta f = f_{1,\text{cal}} - f_{1,\text{obs}}$.

$M (M_{\odot})$	$f_{1,\text{cal}}$ (c day^{-1})	n_p	n_g	l	Δf (c day^{-1})
1.65	20.989	3	15	2	-0.118
1.66	20.874	3	15	2	-0.233
1.67	21.124	3	21	3	0.017
1.68	20.987	3	14	2	-0.120
1.69	21.157	3	8	1	0.050
1.70	21.110	3	20	3	0.003
1.71	21.353	3	13	2	0.246
1.72	20.849	3	8	1	-0.258
1.73	21.139	3	19	3	0.032
1.74	21.016	3	13	2	-0.091
1.75	20.926	3	19	3	-0.181
1.76	21.498	3	18	3	0.391
1.77	21.375	3	18	3	0.268
1.78	21.213	3	12	2	0.106

scattered light contamination or momentum dumps. Similar features have been observed in other HADS stars during the same TESS sector such as TIC 16283570, providing cautious supports to this interpretation.

Furthermore, the analysis reveals that EH Lib is a normal HADS star pulsating in its fundamental mode and locating at the post main sequence stage. This finding is consistent with the tendency proposed by Xue et al. (2018), who suggests that the HADS stars which have left the main sequence and become subgiants with the hydrogen-burning shell, tend to exhibit lower fundamental frequencies as they evolve.

Figure 11 reproduces Figure 9 of Xue et al. (2018), presenting a HR diagram for Delta Scuti stars, with EH Lib plotted by a red star. Table 8 lists the observed fundamental frequencies, the period change rates, and the physical parameters of the best-fit models of these six

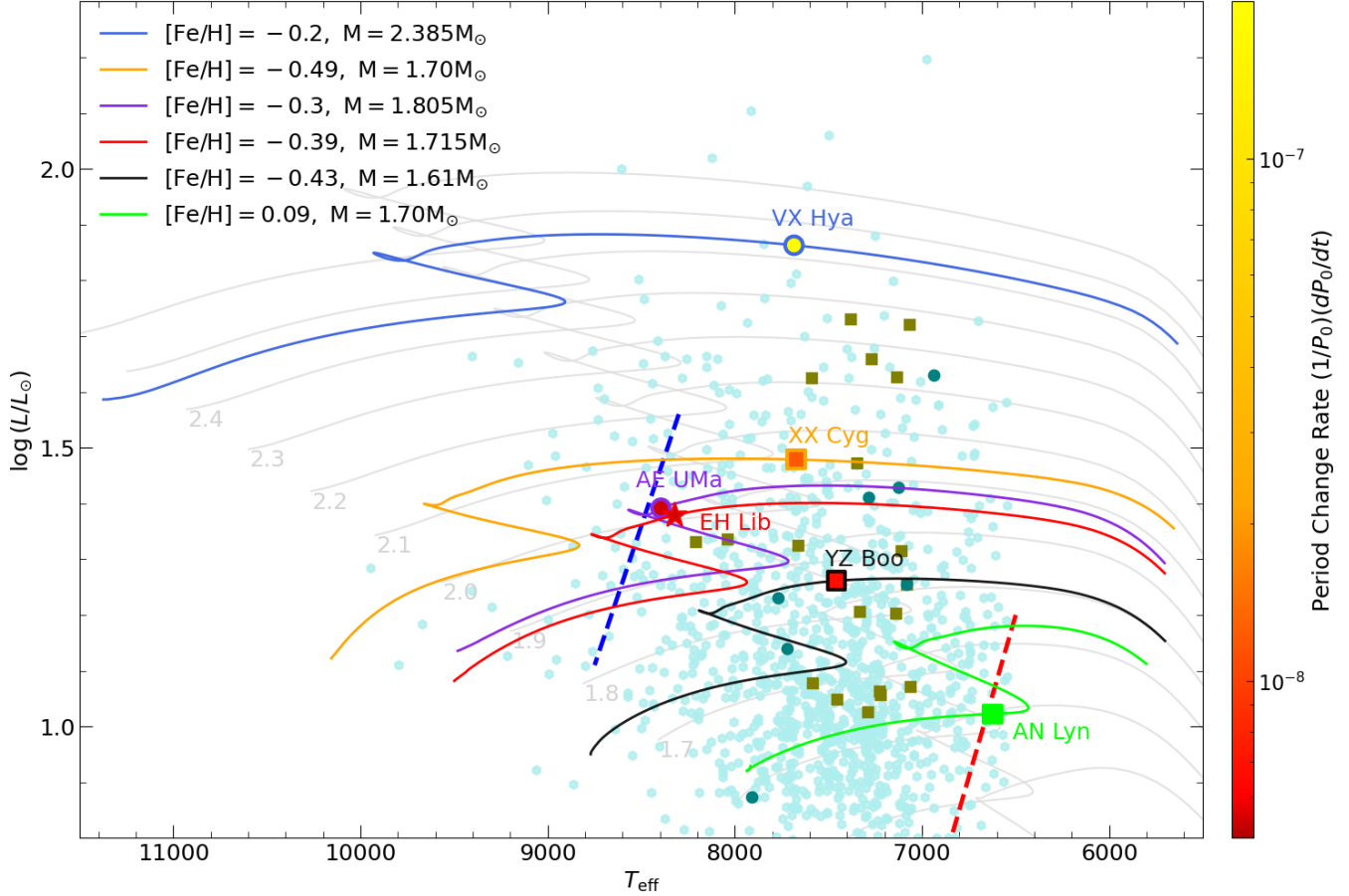


Figure 11. HR diagram for Delta Scuti stars. The best-fit models of six HADS stars studied through asteroseismology are shown with distinct stroke colours and symbols, along with their corresponding evolutionary tracks. Fill colours indicate the period change rates, with redder colour corresponding to shorter rates. See Table 8 for details. Light cyan hexagons present the sample of normal Delta Scuti stars from Murphy et al. (2019), selected based on fractional parallax uncertainties below 3 per cent and pulsation full amplitudes exceeding 0.01 mag. Squares represent single-mode HADS stars, whereas circles represent multi-mode HADS stars. The effective temperatures of the olive and dark cyan data points are derived from the spectral surveys LAMOST (Zhao et al. 2012; Xiang et al. 2015) and GALAH (De Silva et al. 2015; Buder et al. 2021). The luminosities are provided by Gaia DR3 (Gaia Collaboration et al. 2023) and reduced following the method described in Section 3.2. The HADS star sample are taken from an in-house program. To place these stars meaningfully, evolutionary tracks in the mass range 1.4–2.6 M_{\odot} for the ‘standard model’ (Murphy et al. 2019) with the chemical composition ($X = 0.71$, $Z = 0.014$), are computed with MESA. These tracks are shown as grey lines, with labelled masses at the beginnings. The blue and red dash lines mark the boundaries of the theoretical instability strip, derived using time-dependent convection and $\alpha_{MLT} = 1.8$ from Dupret et al. (2005).

HADS stars studied through asteroseismology (Yang et al. 2012; Niu et al. 2017; Li et al. 2018; Xue et al. 2018; Yang et al. 2018). These six HADS stars are found to be slightly evolved, crossing the instability strip. In addition to the trend reported by Xue et al. (2018), it is suggested that the period change rate increases as the stars evolve. Moreover, a comparison between EH Lib and AN Lyn indicates that stars with lower metallicity may evolve more rapidly.

It is noteworthy that EH Lib and AE UMa exhibit consistent period change rates within uncertainties, and possess similar fundamental frequencies and metallicities. Both stars occupy adjacent positions on the HR diagram, having just moved off the main sequence and located near the second turn-offs of their evolutionary tracks. This commonalities raise the question: can these observational parameters alone uniquely determine stellar models for HADS stars? Regrettably, they do not. Despite their comparable bulk properties, their pulsation behaviours differ: EH Lib pulsates in a single mode, whereas AE UMa pulsates in two modes. This discrepancy implies that our understanding of the internal physics of HADS stars remains incomplete. Nonetheless, it is fortuitous that both stars reside in the Hertzsprung

gap, a sparsely populated region of the HR diagram. Consequently, further investigation of these analogue HADS stars may provide an invaluable natural laboratory for understanding stellar evolution theories during this transitional phase.

6 CONCLUSIONS

Through the analysis of space-based photometry from the TESS mission, we extract 17 significant frequencies, comprising f_0 , f_1 and f_2 , in addition to the harmonics of f_0 and a linear combination, and determine 158 times of maximum light. Ground-based photometric data collected in the V and R bands between 2009 and 2018 provide additional 91 times of maximum light. Based on the pulsation constant and P-L relations, f_0 is identified as the fundamental radial pulsation mode.

The classical O-C method is utilized to estimate the period change rate of EH Lib. The period change rate of the fundamental mode which is consistent with that of the star, is determined as

Table 8. The observed frequencies of the fundamental mode, period change rates and physical parameters of the best-fit models of six HADS stars studied through asteroseismology.

Star	f_0 (c day $^{-1}$)	$(1/P_0)(dP_0/dt)$ (yr $^{-1}$)	M/M_\odot	Age (10 9 years)	[Fe/H]	Reference
VX Hya	4.4763	$1.81(\pm 0.09) \times 10^{-7}$	2.385	0.43	-0.2	Xue et al. (2018)
XX Cyg	7.4148	$1.19(\pm 0.13) \times 10^{-8}$	1.70	0.9	-0.49	Yang et al. (2012)
YZ Boo	9.6069	$6.7(\pm 0.9) \times 10^{-9}$	1.61	1.44	-0.43	Yang et al. (2018)
AN Lyn	10.1721		1.70	1.33	0.09	Li et al. (2018)
EH Lib	11.3105	$5.4(\pm 0.5) \times 10^{-9}$	1.715	1.14	-0.39	this work
AE UMa	11.6256	$5.4(\pm 1.9) \times 10^{-9}$	1.805	1.055	-0.3	Niu et al. (2017)

$(1/P_0)(dP_0/dt) = (5.4 \pm 0.5) \times 10^{-9}$ yr $^{-1}$, based on 342 times of maximum light spanning over 70 years. Additionally, a new ephemeris is derived:

$$C = BJD\ 2435223.7596 + 0.088413248 \times E + 5.76 \times 10^{-14} E^2$$

The stellar evolutionary models are constructed with initial masses ranging from $1.50 M_\odot$ to $2.50 M_\odot$ and the metal abundance $Z = 0.006$. By constraining these models using the observed f_0 and $(1/P_0)(dP_0/dt)$ within respective uncertainties, we determine the stellar parameters of EH Lib (see Table 6). The results indicate that EH Lib is a single-mode HADS star, locating at the post main sequence stage, or more accurately, in the Hertzsprung gap, with a helium core and a hydrogen-burning shell.

Furthermore, we would like to emphasize that: (a) for EH Lib, the period change rate can be attributed to stellar evolutionary effects; (b) this study of EH Lib confirms that constraining stellar models for HADS stars using both frequencies and period change rates is feasible; (c) the determined position of EH Lib on the HR diagram indicates that it is in the post main sequence stage, consistent with the general consensus for HADS stars; (d) this study of EH Lib, which is an analogue of AE UMa in the region Hertzsprung gap, expands the current limited sample of HADS stars studied through asteroseismology. It lays the groundwork for future studies of their commonalities and specific properties to deepen our understanding of HADS stars.

ACKNOWLEDGEMENTS

JNF acknowledges the support from the National Natural Science Foundation of China (NSFC) through the grants 12090040, 12090042 and 12427804. This work is supported by the China Manned Space Program with grant no. CMS-CSST-2025-A013, and the Central Guidance for Local Science and Technology Development Fund under No. ZYYD2025QY27. LFM has received financial support from the UNAM via PAPIIT IN117323. JS acknowledges the support from the International Centre of Supernovae, Yunnan Key Laboratory (No. 202302AN360001) and the West Light Foundation of the Chinese Academy of Sciences. This work is based upon observations carried out at the Yunnan Astronomical Observatory of China, Xinglong station of National Astronomical Observatories of China, and Observatorio Astronómico Nacional on the Sierra San Pedro Mártir (OAN-SPM), Baja California, México. We thank the technical staff and night assistants for facilitating and helping making the observations. This work makes use of data collected by the TESS mission, which are publicly available from the Mikulski Archive for Space Telescopes (MAST, <https://archive.stsci.edu>). Funding for the TESS mission is provided by NASA's Science Mission directorate. This work also

includes data from the European Space Agency (ESA) mission Gaia, (<https://www.cosmos.esa.int/gaia>), processed by the Gaia Data Processing and Analysis Consortium (DPAC, <https://www.cosmos.esa.int/web/gaia/dpac/consortium>). Funding for the DPAC has been provided by national institutions, in particular the institutions participating in the Gaia Multilateral Agreement. This research made use of Lightkurve, a Python package for Kepler and TESS data analysis. We gratefully acknowledge them for making such high-quality data available. Finally, we are indebted to Dr. Filiz Kahraman Aliçavuş for insightful discussions on the spectroscopic data and to Dr. Timothy R. Bedding as well as Dr. Tianqi Cang for valuable suggestions on this manuscript.

software: IRAF (Tody 1986, 1993), AstroImageJ (Collins et al. 2017), Period04 (Lenz & Breger 2005), MESA (Paxton et al. 2011, 2013, 2015, 2018, 2019; Jermyn et al. 2023), GYRE (Townsend & Teitler 2013; Townsend et al. 2018; Goldstein & Townsend 2020).

DATA AVAILABILITY

The data underlying the research results of this article are available upon reasonable request to the corresponding author.

REFERENCES

- Aerts C., 2021, *Reviews of Modern Physics*, **93**, 015001
- Aerts C., Christensen-Dalsgaard J., Kurtz D. W., 2010, Asteroseismology. Springer, doi:10.1007/978-1-4020-5803-5
- Andrae R., et al., 2018, *A&A*, **616**, A8
- Ashbrook J., 1952, *AJ*, **57**, 64
- Balona L. A., 1994, *MNRAS*, **268**, 119
- Balona L. A., et al., 2012, *MNRAS*, **419**, 3028
- Barac N., Bedding T. R., Murphy S. J., Hey D. R., 2022, *MNRAS*, **516**, 2080
- Baran A. S., Koen C., 2021, *Acta Astron.*, **71**, 113
- Barentsen G., et al., 2021, lightkurve/lightkurve: Lightkurve v2.0.9, doi:10.5281/zenodo.1181928
- Bedding T. R., et al., 2020, *Nature*, **581**, 147
- Breger M., 1979, *PASP*, **91**, 5
- Breger M., 1990, Delta Scuti Star Newsletter, **2**, 13
- Breger M., 2000, in Breger M., Montgomery M., eds, Astronomical Society of the Pacific Conference Series Vol. 210, Delta Scuti and Related Stars. p. 3
- Breger M., Bregman J. N., 1975, *ApJ*, **200**, 343
- Breger M., Pamyatnykh A. A., 1998, *A&A*, **332**, 958
- Bressan A., Marigo P., Girardi L., Salasnich B., Dal Cero C., Rubele S., Nanni A., 2012, *MNRAS*, **427**, 127
- Buder S., et al., 2021, *MNRAS*, **506**, 150
- Code A. D., 1950, *PASP*, **62**, 166
- Collins K. A., Kielkopf J. F., Stassun K. G., Hessman F. V., 2017, *AJ*, **153**, 77
- Daszyńska-Daszkiewicz J., Walczak P., Pamyatnykh A. A., Szewczuk W., 2022, *MNRAS*, **512**, 3551

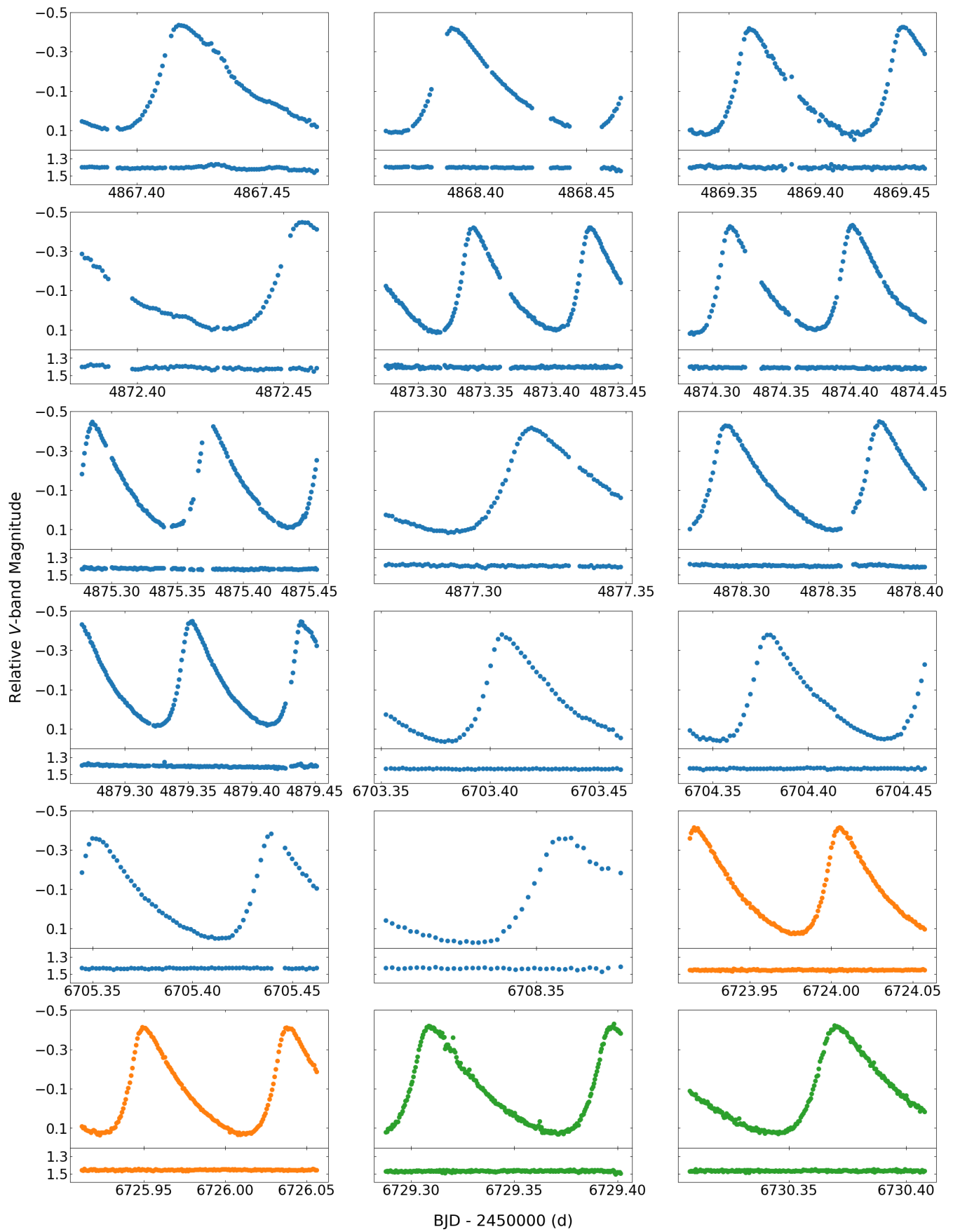
- De Silva G. M., et al., 2015, *MNRAS*, **449**, 2604
- Dupret M. A., Grigahcène A., Garrido R., Gabriel M., Scuflaire R., 2005, *A&A*, **435**, 927
- Fitch W. S., 1957, *AJ*, **62**, 108
- Fitch W. S., Wisniewski W. Z., Johnson H. L., 1966, Communications of the Lunar and Planetary Laboratory, **5**, 3
- Fu J. N., et al., 2008, *AJ*, **135**, 1958
- Fu J. N., et al., 2009, *PASP*, **121**, 251
- Fu J. N., et al., 2013, *MNRAS*, **429**, 1585
- Gaia Collaboration et al., 2023, *A&A*, **674**, A1
- Garrido R., Alfaro E. J., Quintana J. M., Saez M., 1979, *A&AS*, **36**, 51
- Goldstein J., Townsend R. H. D., 2020, *ApJ*, **899**, 116
- Goupil M. J., Dupret M. A., Samadi R., Boehm T., Alecian E., Suarez J. C., Lebreton Y., Catala C., 2005, *Journal of Astrophysics and Astronomy*, **26**, 249
- Green G. M., Schlafly E., Zucker C., Speagle J. S., Finkbeiner D., 2019, *ApJ*, **887**, 93
- Hamdy M. A., 1985, Information Bulletin on Variable Stars, **2810**, 1
- Handler G., 2009, in Guzik J. A., Bradley P. A., eds, American Institute of Physics Conference Series Vol. 1170, Stellar Pulsation: Challenges for Theory and Observation. AIP, pp 403–409 ([arXiv:2110.09806](https://arxiv.org/abs/2110.09806)), doi:10.1063/1.3246528
- Harris F. J., 1978, IEEE Proceedings, **66**, 51
- Holdsworth D. L., et al., 2014, *MNRAS*, **439**, 2078
- Jayasinghe T., et al., 2020, *MNRAS*, **493**, 4186
- Jermyn A. S., et al., 2023, *ApJS*, **265**, 15
- Jiang S. Y., Yang Z. Z., 1981, Acta Astronomica Sinica, **22**, 279
- Joner M. D., 1986, *PASP*, **98**, 651
- Jordi C., et al., 2010, *A&A*, **523**, A48
- Kahraman Aliçavuş F., Niemczura E., Polińska M., Helminiak K. G., Lampens P., Molenda-Żakowicz J., Ukita N., Kambe E., 2017, *MNRAS*, **470**, 4408
- Karetnikov V. G., Medvedev Y. A., 1977, Information Bulletin on Variable Stars, **1310**, 1
- Kervella P., Arenou F., Mignard F., Thévenin F., 2019, *A&A*, **623**, A72
- Kippenhahn R., Weigert A., Weiss A., 2013, Stellar Structure and Evolution. Springer, doi:10.1007/978-3-642-30304-3
- Kurtz D. W., 2022, *ARA&A*, **60**, 31
- Lee Y.-H., Kim S. S., Shin J., Lee J., Jin H., 2008, *PASJ*, **60**, 551
- Lenz P., Breger M., 2005, *Communications in Astroseismology*, **146**, 53
- Li G., Fu J., Su J., Fox-Machado L., Michel R., Guo Z., Liu J., Feng G., 2018, *MNRAS*, **473**, 398
- Lightkurve Collaboration et al., 2018, Lightkurve: Kepler and TESS time series analysis in Python, Astrophysics Source Code Library, record ascl:1812.013
- Mahdy H. A., Szeidl B., 1980, Communications of the Konkoly Observatory Hungary, **74**, 1
- Mamajek E. E., et al., 2015, arXiv e-prints, p. arXiv:1510.06262
- McNamara D. H., 2000, in Breger M., Montgomery M., eds, Astronomical Society of the Pacific Conference Series Vol. 210, Delta Scuti and Related Stars. p. 373
- Murphy S. J., Hey D., Van Reeth T., Bedding T. R., 2019, *MNRAS*, **485**, 2380
- Netzel H., Pietrukowicz P., Soszyński I., Wrona M., 2022, *MNRAS*, **510**, 1748
- Niu J.-S., Xue H.-F., 2022, *ApJ*, **938**, L20
- Niu J.-S., Xue H.-F., 2024, *A&A*, **682**, L8
- Niu J.-S., et al., 2017, *MNRAS*, **467**, 3122
- Oosterhoff P. T., Walraven T., 1966, Bull. Astron. Inst. Netherlands, **18**, 387
- Paxton B., Bildsten L., Dotter A., Herwig F., Lesaffre P., Timmes F., 2011, *ApJS*, **192**, 3
- Paxton B., et al., 2013, *ApJS*, **208**, 4
- Paxton B., et al., 2015, *ApJS*, **220**, 15
- Paxton B., et al., 2018, *ApJS*, **234**, 34
- Paxton B., et al., 2019, *ApJS*, **243**, 10
- Pena J. H., Villarreal C., Pina D. S., Renteria A., Soni A., Guillen J., Calderon J., 2017, Information Bulletin on Variable Stars, **6231**, 1
- Petersen J. O., Christensen-Dalsgaard J., 1996, *A&A*, **312**, 463
- Poro A., et al., 2021, *PASP*, **133**, 084201
- Ricker G. R., et al., 2014, in Oschmann Jacobus M. J., Clampin M., Fazio G. G., MacEwen H. A., eds, Society of Photo-Optical Instrumentation Engineers (SPIE) Conference Series Vol. 9143, Space Telescopes and Instrumentation 2014: Optical, Infrared, and Millimeter Wave. p. 914320 ([arXiv:1406.0151](https://arxiv.org/abs/1406.0151)), doi:10.1117/12.2063489
- Ricker G. R., et al., 2015, *Journal of Astronomical Telescopes, Instruments, and Systems*, **1**, 014003
- Rodríguez E., Breger M., 2001, *A&A*, **366**, 178
- Sanwal N. B., Pande M. C., 1961, The Observatory, **81**, 199
- Solano E., Fernley J., 1997, *A&AS*, **122**, 131
- Sterken C., 2005, in Sterken C., ed., Astronomical Society of the Pacific Conference Series Vol. 335, The Light-Time Effect in Astrophysics: Causes and cures of the O-C diagram. p. 3
- Templeton M., Basu S., Demarque P., 2002, *ApJ*, **576**, 963
- Tody D., 1986, in Crawford D. L., ed., Society of Photo-Optical Instrumentation Engineers (SPIE) Conference Series Vol. 627, Instrumentation in astronomy VI. p. 733, doi:10.1117/12.968154
- Tody D., 1993, in Hanisch R. J., Brissenden R. J. V., Barnes J., eds, Astronomical Society of the Pacific Conference Series Vol. 52, Astronomical Data Analysis Software and Systems II. p. 173
- Townsend R. H. D., Teitler S. A., 2013, *MNRAS*, **435**, 3406
- Townsend R. H. D., Goldstein J., Zweibel E. G., 2018, *MNRAS*, **475**, 879
- Uytterhoeven K., et al., 2011, *A&A*, **534**, A125
- Wang J., Fu J.-N., Zong W., Wang J., Zhang B., 2021, *MNRAS*, **506**, 6117
- Wenger M., et al., 2000, *A&AS*, **143**, 9
- Xiang M. S., et al., 2015, *MNRAS*, **448**, 822
- Xue H.-F., Niu J.-S., 2020, *ApJ*, **904**, 5
- Xue H.-F., et al., 2018, *ApJ*, **861**, 96
- Yang D., Tang Q., Jiang S., 1992, Information Bulletin on Variable Stars, **3769**, 1
- Yang X. H., Fu J. N., Zha Q., 2012, *AJ*, **144**, 92
- Yang T.-Z., Esamdin A., Fu J.-N., Niu H.-B., Feng G.-J., Song F.-F., Liu J.-Z., Ma L., 2018, *Research in Astronomy and Astrophysics*, **18**, 002
- Zhao G., Zhao Y.-H., Chu Y.-Q., Jing Y.-P., Deng L.-C., 2012, *Research in Astronomy and Astrophysics*, **12**, 723
- Ziaali E., Bedding T. R., Murphy S. J., Van Reeth T., Hey D. R., 2019, *MNRAS*, **486**, 4348

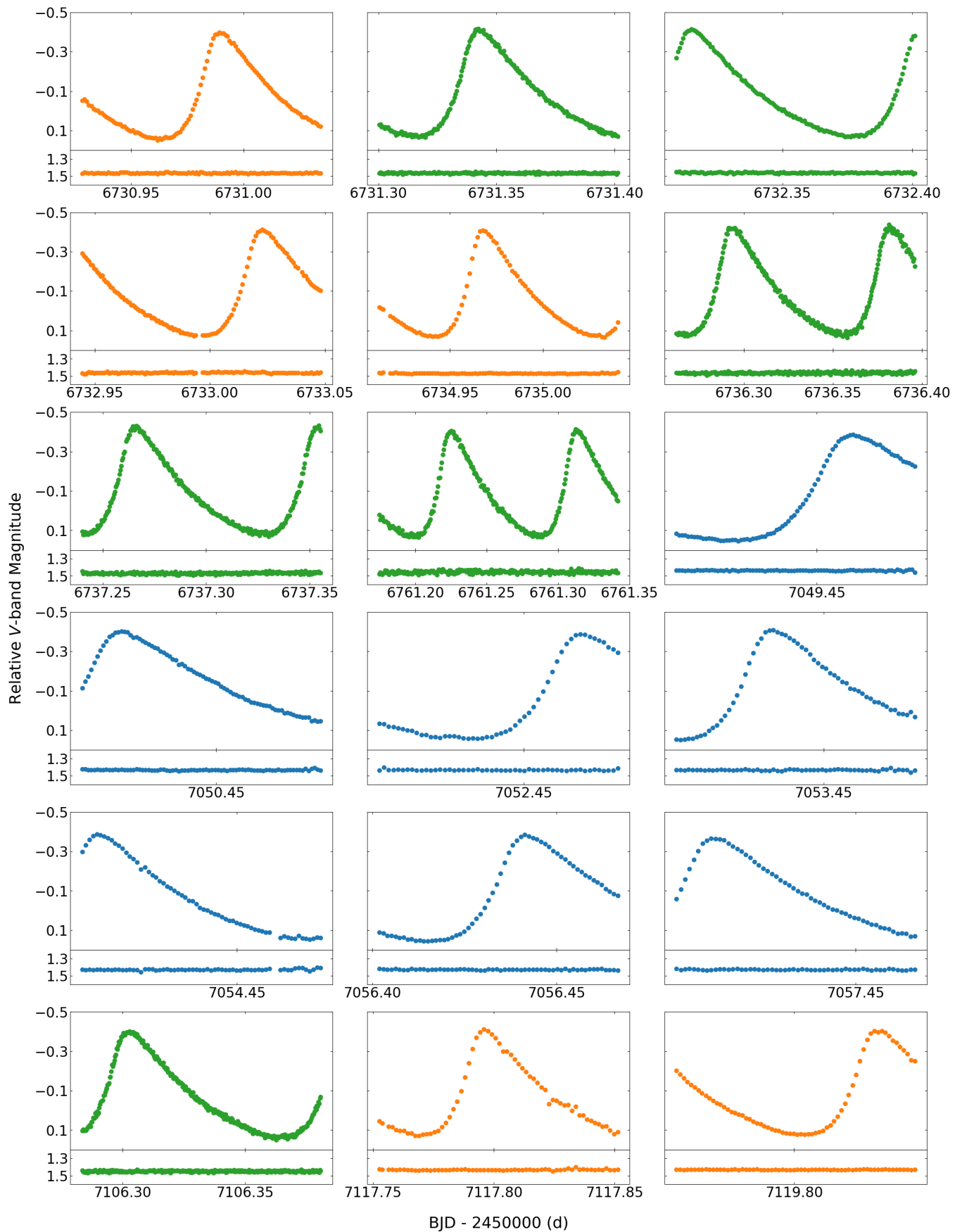
APPENDIX A:

Figures A1 and A2 display the whole resulting light curves after data reduction from the ground-based observations between 2009 and 2018 in *V* and *R* bands, respectively.

Tables A1, A2 and A3 present the times of maximum light for EH Lib derived from new ground-based R-band observations, TESS observations, and previous literature, respectively.

This paper has been typeset from a \TeX / \LaTeX file prepared by the author.





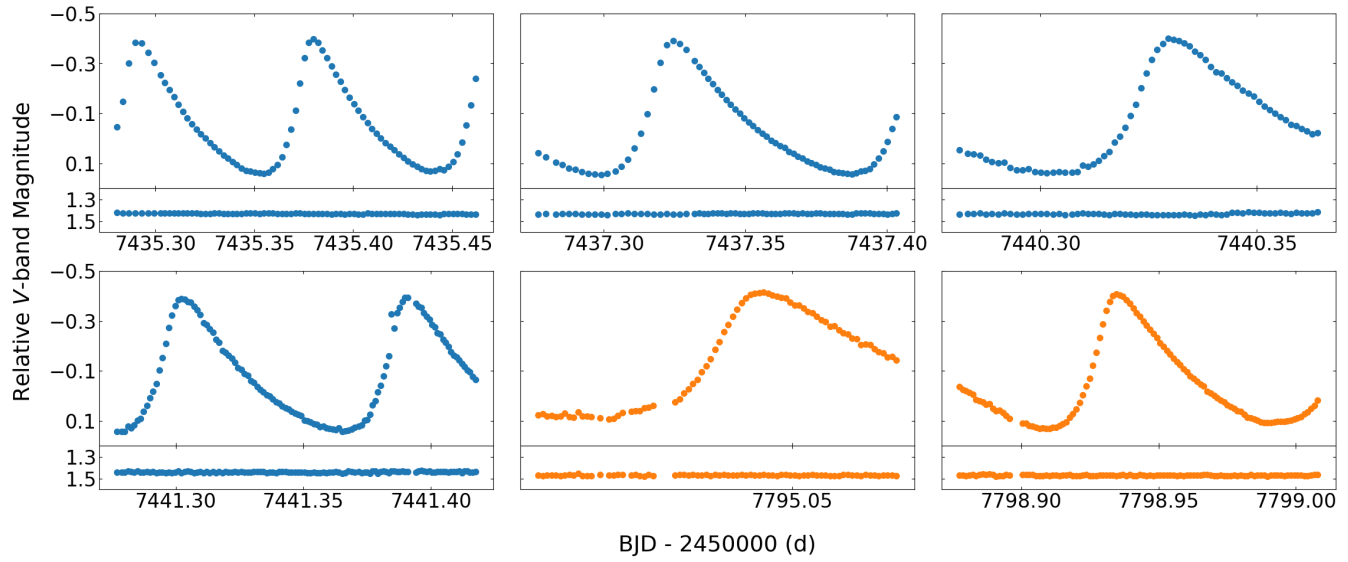
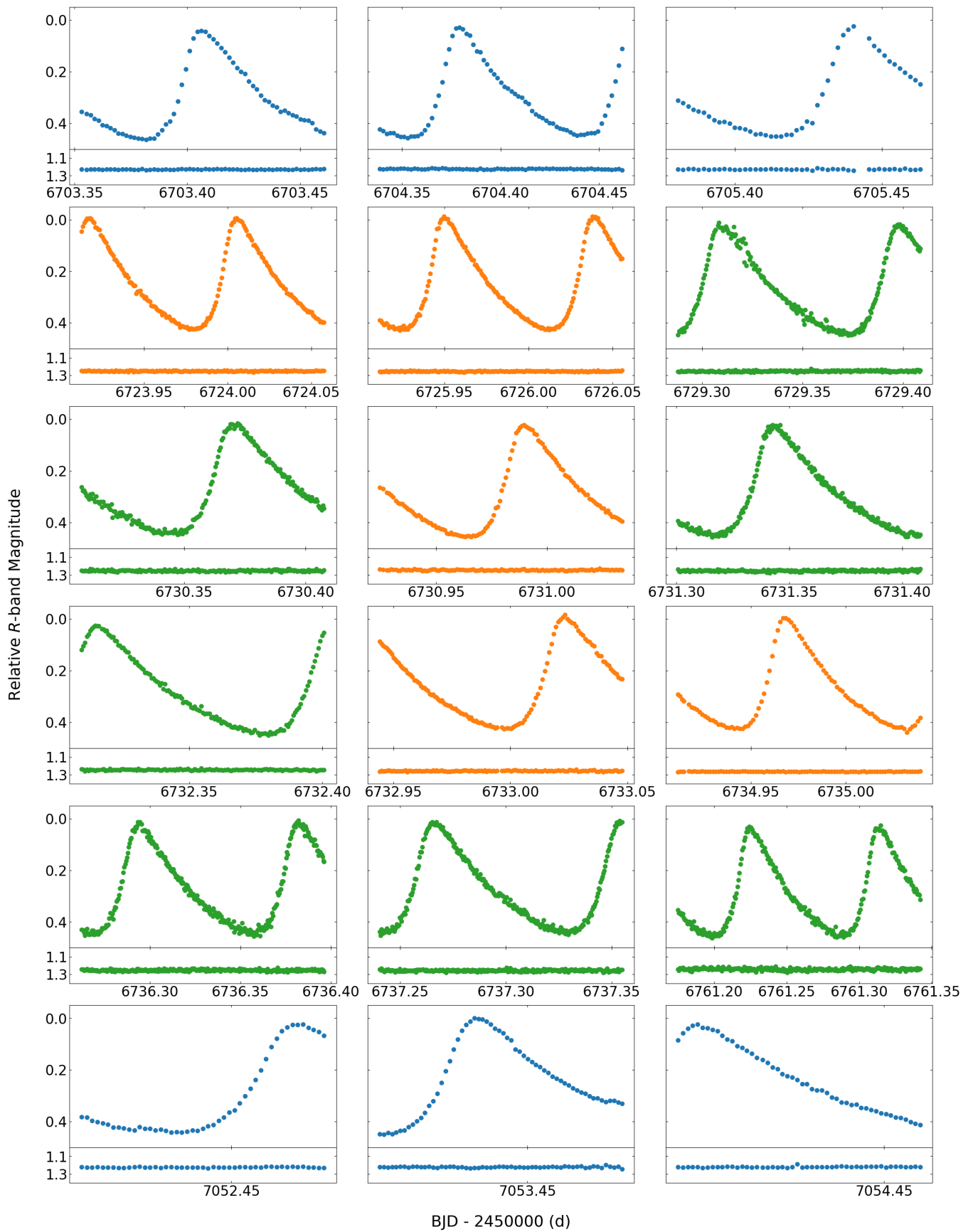


Figure A1. The light curves of EH Lib in V -band observed between 2009 and 2018. In each subfigure, the upper panel shows the magnitude differences between EH Lib and the comparison star, and the bottom panel shows the magnitude differences between the check star and the comparison star. Outliers are removed. The blue points come from the observations with the 101.6-cm Telescope at Yunnan Astronomical Observatory of China, the orange ones from those with the 84-cm Telescope at National Astronomical Observatory San Pedro M  rtir of Mexico, the green ones from those with the 85-cm Telescope at Xinglong Station, and the red ones from those with the Xinglong 2.16-m Telescope.



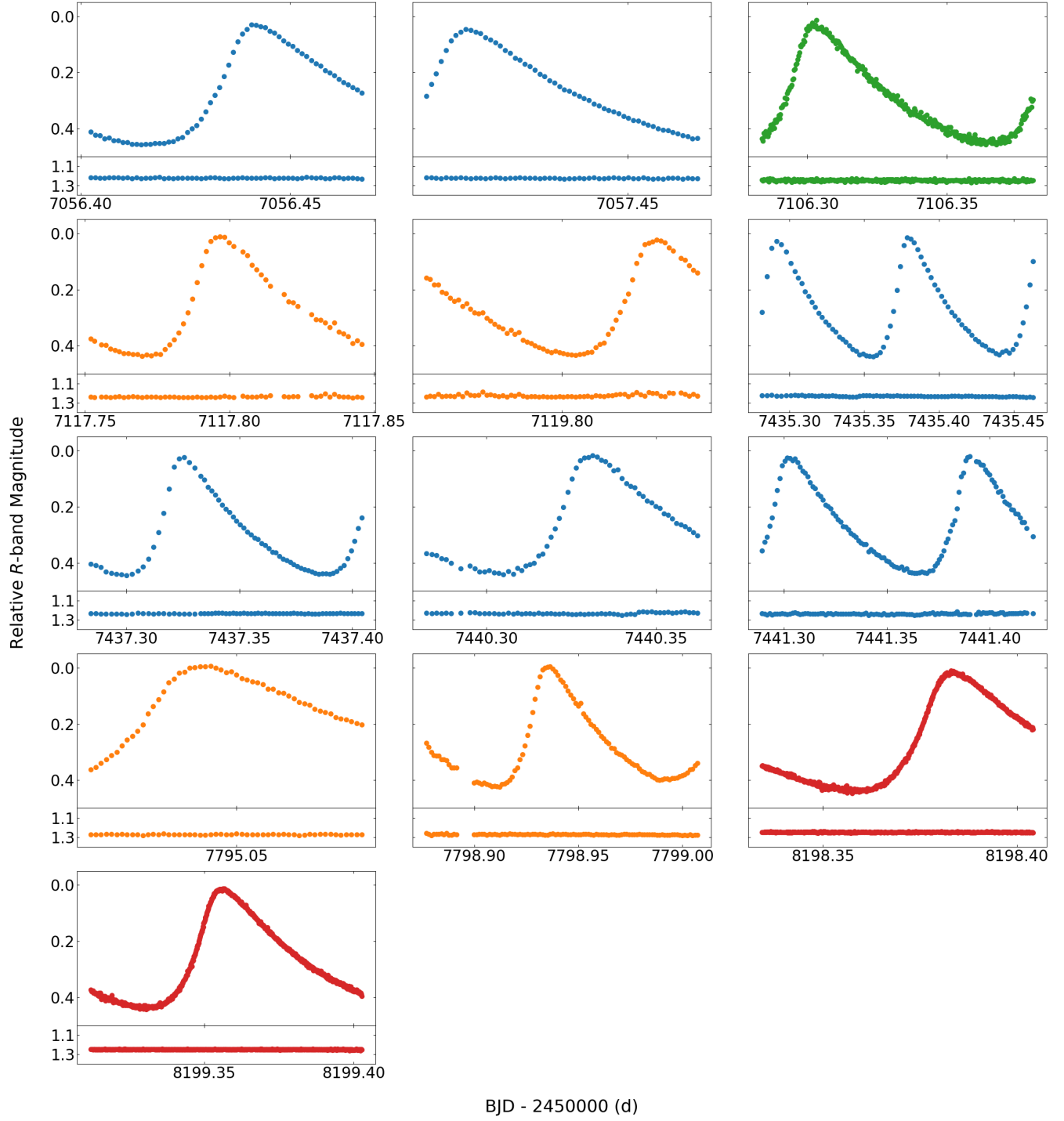


Figure A2. The light curves of EH Lib in R -band observed between 2009 and 2018. In each subfigure, the upper panel shows the magnitude differences between EH Lib and the comparison star, and the bottom panel shows the magnitude differences between the check star and the comparison star. Outliers are removed. The blue points come from the observations with the 101.6-cm Telescope at Yunnan Astronomical Observatory of China, the orange ones from those with the 84-cm Telescope at National Astronomical Observatory San Pedro Martir of Mexico, the green ones from those with the 85-cm Telescope at Xinglong Station, and the red ones from those with the Xinglong 2.16-m Telescope.

Table A1. Times of maximum light of EH Lib from new ground-based R -band observations. T_{\max} is in BJD-2450000, O-C is in days. Epoch and O-C are derived from the ephemeris formula in Equation (8).

T_{\max}	Epoch	O-C	T_{\max}	Epoch	O-C	T_{\max}	Epoch	O-C	T_{\max}	Epoch	O-C
6703.40821	242946	-0.00005	6730.99405	243258	0.00085	7052.46364	246894	-0.00021	7437.32783	251247	0.00104
6704.38111	242957	0.00030	6731.34709	243262	0.00024	7053.43703	246905	0.00064	7440.33358	251281	0.00073
6705.44244	242969	0.00067	6732.32008	243273	0.00068	7054.40930	246916	0.00036	7441.30600	251292	0.00061
6723.92075	243178	0.00061	6733.02777	243281	0.00106	7056.44270	246939	0.00026	7441.39419	251293	0.00038
6724.00923	243179	0.00067	6734.97284	243303	0.00104	7057.41543	246950	0.00044	7795.04718	255293	0.00031
6725.95418	243201	0.00053	6736.29821	243318	0.00021	7106.30795	247503	0.00042	7798.93725	255337	0.00019
6726.04259	243202	0.00053	6736.38675	243319	0.00034	7117.80261	247633	0.00136	8198.38830	259855	0.00010
6729.31379	243239	0.00044	6737.27107	243329	0.00053	7119.83577	247656	0.00101	8199.36076	259866	0.00001
6729.40208	243240	0.00032	6761.23047	243600	-0.00007	7435.29462	251224	0.00133			
6730.37518	243251	0.00086	6761.31932	243601	0.00037	7435.38199	251225	0.00029			

Table A2. Times of maximum light of EH Lib from TESS observations. T_{\max} is in BJD-2450000, O-C is in days. Epoch and O-C are derived from the ephemeris formula in Equation (8).

T_{\max}	Epoch	O-C									
9693.01456	276760	0.00008	9700.35275	276843	-0.00003	9703.88934	276883	0.00003	9714.23368	277000	0.00002
9693.10299	276761	0.00010	9700.44118	276844	-0.00001	9703.97777	276884	0.00005	9714.32211	277001	0.00004
9693.19126	276762	-0.00004	9700.52960	276845	0.00000	9704.06604	276885	-0.00009	9714.41053	277002	0.00005
9693.27969	276763	-0.00003	9700.61803	276846	0.00001	9704.15447	276886	-0.00008	9714.49896	277003	0.00006
9693.36811	276764	-0.00002	9700.70646	276847	0.00003	9704.24305	276887	0.00009	9714.58738	277004	0.00007
9693.45654	276765	0.00000	9700.79488	276848	0.00004	9704.33132	276888	-0.00006	9714.67565	277005	-0.00007
9693.54497	276766	0.00001	9700.88315	276849	-0.00010	9704.41974	276889	-0.00004	9714.76408	277006	-0.00006
9693.63339	276767	0.00003	9700.97158	276850	-0.00009	9704.50832	276890	0.00012	9714.85250	277007	-0.00005
9693.72182	276768	0.00004	9701.06001	276851	-0.00007	9704.59675	276891	0.00014	9714.94108	277008	0.00011
9693.81009	276769	-0.00010	9701.14859	276852	0.00009	9704.68518	276892	0.00015	9715.02950	277009	0.00013
9693.89883	276770	0.00022	9701.23701	276853	0.00011	9705.92282	276906	0.00001	9715.11777	277010	-0.00002
9693.98710	276771	0.00008	9701.32544	276854	0.00012	9706.01125	276907	0.00002	9715.20620	277011	-0.00001
9694.07537	276772	-0.00006	9701.41371	276855	-0.00002	9706.09967	276908	0.00003	9715.29462	277012	0.00001
9694.16395	276773	0.00011	9701.50229	276856	0.00015	9706.18810	276909	0.00005	9715.38305	277013	0.00002
9698.05397	276817	-0.00007	9701.59057	276857	0.00000	9706.27652	276910	0.00006	9715.47147	277014	0.00003
9698.14255	276818	0.00010	9701.67899	276858	0.00002	9706.36479	276911	-0.00009	9715.55990	277015	0.00004
9698.23082	276819	-0.00004	9701.76742	276859	0.00003	9706.45337	276912	0.00008	9715.64832	277016	0.00005
9698.31925	276820	-0.00003	9701.85569	276860	-0.00011	9706.54180	276913	0.00009	9715.73675	277017	0.00006
9698.40767	276821	-0.00001	9701.94427	276861	0.00006	9706.63022	276914	0.00010	9715.82517	277018	0.00007
9698.49625	276822	0.00016	9702.03254	276862	-0.00008	9706.71849	276915	-0.00004	9715.91359	277019	0.00008
9698.58468	276823	0.00017	9702.12112	276863	0.00008	9706.80707	276916	0.00013	9716.00202	277020	0.00009
9698.67295	276824	0.00003	9702.20955	276864	0.00010	9706.89534	276917	-0.00002	9716.09029	277021	-0.00005
9698.76138	276825	0.00004	9702.29782	276865	-0.00004	9706.98377	276918	0.00000	9716.17871	277022	-0.00004
9698.84965	276826	-0.00010	9702.38625	276866	-0.00003	9707.07235	276919	0.00016	9716.26714	277023	-0.00003
9698.93808	276827	-0.00009	9702.47468	276867	-0.00002	9707.16062	276920	0.00002	9716.35556	277024	-0.00002
9699.02650	276828	-0.00007	9702.56326	276868	0.00015	9707.24920	276921	0.00019	9716.44399	277025	0.00000
9699.11493	276829	-0.00006	9702.65153	276869	0.00001	9712.90747	276985	0.00001	9716.53241	277026	0.00001
9699.20351	276830	0.00011	9702.73980	276870	-0.00013	9712.99589	276986	0.00002	9716.62084	277027	0.00002
9699.29194	276831	0.00012	9702.82823	276871	-0.00012	9713.08416	276987	-0.00012	9716.70911	277028	-0.00012
9699.38021	276832	-0.00002	9702.91681	276872	0.00005	9713.17274	276988	0.00004	9716.79753	277029	-0.00011
9699.46848	276833	-0.00016	9703.00523	276873	0.00006	9713.26117	276989	0.00005	9716.88611	277030	0.00005
9699.55706	276834	0.00001	9703.09366	276874	0.00007	9713.34959	276990	0.00006	9716.97438	277031	-0.00009
9699.64549	276835	0.00002	9703.18209	276875	0.00009	9713.43786	276991	-0.00008	9717.06311	277032	0.00023
9699.73392	276836	0.00003	9703.27051	276876	0.00010	9713.52613	276992	-0.00022	9717.15138	277033	0.00008
9699.82234	276837	0.00005	9703.35894	276877	0.00011	9713.61471	276993	-0.00006	9717.23965	277034	-0.00006
9699.91077	276838	0.00006	9703.44736	276878	0.00012	9713.70329	276994	0.00011	9717.32823	277035	0.00011
9699.99920	276839	0.00007	9703.53564	276879	-0.00002	9713.79156	276995	-0.00003	9717.41650	277036	-0.00004
9700.08747	276840	-0.00007	9703.62406	276880	0.00000	9713.87998	276996	-0.00002	9717.50492	277037	-0.00003
9700.17590	276841	-0.00005	9703.71264	276881	0.00016	9713.96825	276997	-0.00016			
9700.26432	276842	-0.00004	9703.80092	276882	0.00002	9714.14526	276999	0.00001			

Table A3. Times of maximum light of EH Lib reported in previous literature. T_{\max} is in BJD-2400000, O-C is in days. Epoch and O-C are derived from the ephemeris formula in Equation (8). Det: detector (pg=photograph, pe=photoelectric photometer).

T_{\max}	Epoch	O-C	Det.	Reference	T_{\max}	Epoch	O-C	Det.	Reference
33438.60796	-20191	0.00154	pe	Code (1950)	43254.60017	90833	-0.00081	pe	Garrido et al. (1979)
33711.71687	-17102	0.00186	pg	Ashbrook (1952)	43255.57337	90844	-0.00016	pe	Garrido et al. (1979)
33737.70937	-16808	0.00086	pg	Ashbrook (1952)	43255.66187	90845	-0.00007	pe	Garrido et al. (1979)
33743.72237	-16740	0.00176	pg	Ashbrook (1952)	43256.63347	90856	-0.00102	pe	Garrido et al. (1979)
35223.75995	0	0.00125	pe	Fitch (1957)	43274.58127	91059	-0.00111	pe	Garrido et al. (1979)
35223.84815	1	0.00104	pe	Fitch (1957)	43287.57837	91206	-0.00076	pe	Garrido et al. (1979)
35223.93755	2	0.00203	pe	Fitch (1957)	43957.57376	98784	-0.00110	pe	Mahdy & Szeidl (1980)
35225.79355	23	0.00135	pe	Fitch (1957)	44378.15586	103541	-0.00092	pe	Jiang & Yang (1981)
35243.74175	226	0.00165	pe	Fitch (1957)	44379.12926	103552	-0.00007	pe	Jiang & Yang (1981)
35243.83015	227	0.00164	pe	Fitch (1957)	44379.21766	103553	-0.00008	pe	Jiang & Yang (1981)
35622.68024	4512	0.00088	pe	Fitch (1957)	44406.09416	103857	-0.00122	pe	Jiang & Yang (1981)
35622.76894	4513	0.00116	pe	Fitch (1957)	44406.18316	103858	-0.00063	pe	Jiang & Yang (1981)
36996.44464	20050	-0.00006	pe	Sanwal & Pande (1961)	44620.40855	106281	-0.00058	pe	Jiang & Yang (1981)
37054.26775	20704	0.00077	pe	Sanwal & Pande (1961)	45433.98716	115483	-0.00085	pe	Joner (1986)
37054.35555	20705	0.00015	pe	Sanwal & Pande (1961)	45439.91076	115550	-0.00094	pe	Joner (1986)
37075.22255	20941	0.00162	pe	Sanwal & Pande (1961)	45440.97156	115562	-0.00110	pe	Joner (1986)
37075.31125	20942	0.00191	pe	Sanwal & Pande (1961)	45441.94436	115573	-0.00084	pe	Joner (1986)
37075.39855	20943	0.00080	pe	Sanwal & Pande (1961)	45458.91976	115765	-0.00079	pe	Joner (1986)
37077.16735	20963	0.00133	pe	Sanwal & Pande (1961)	45477.75166	115978	-0.00092	pe	Joner (1986)
37082.20575	21020	0.00018	pe	Sanwal & Pande (1961)	45477.84036	115979	-0.00063	pe	Joner (1986)
37105.19305	21280	0.00003	pe	Sanwal & Pande (1961)	45519.74828	116453	-0.00061	pe	Joner (1986)
37114.30135	21383	0.00176	pe	Oosterhoff & Walraven (1966)	45520.72008	116464	-0.00135	pe	Joner (1986)
37116.24535	21405	0.00067	pe	Oosterhoff & Walraven (1966)	46094.34669	122952	-0.00001	pe	Yang et al. (1992)
37116.33435	21406	0.00126	pe	Oosterhoff & Walraven (1966)	46095.31889	122963	-0.00036	pe	Yang et al. (1992)
37403.32207	24652	-0.00049	pe	Sanwal & Pande (1961)	46095.40759	122964	-0.00007	pe	Yang et al. (1992)
37403.41187	24653	0.00090	pe	Sanwal & Pande (1961)	46146.50910	123542	-0.00144	pe	Hamdy (1985)
37408.36277	24709	0.00065	pe	Sanwal & Pande (1961)	46146.59730	123543	-0.00165	pe	Hamdy (1985)
37410.30777	24731	0.00056	pe	Sanwal & Pande (1961)	46147.48190	123553	-0.00118	pe	Hamdy (1985)
37412.34057	24754	-0.00014	pe	Sanwal & Pande (1961)	46147.57010	123554	-0.00139	pe	Hamdy (1985)
38441.03042	36389	0.00135	pe	Fitch et al. (1966)	46148.45410	123564	-0.00153	pe	Hamdy (1985)
38467.02292	36683	0.00035	pe	Fitch et al. (1966)	46148.54250	123565	-0.00154	pe	Hamdy (1985)
41476.43317	70721	-0.00018	pe	Mahdy & Szeidl (1980)	46151.54870	123599	-0.00139	pe	Hamdy (1985)
42159.51343	78447	-0.00083	pe	Mahdy & Szeidl (1980)	46179.04430	123910	-0.00232	pe	Yang et al. (1992)
42162.51863	78481	-0.00168	pe	Karetnikov & Medvedev (1977)	46179.13370	123911	-0.00133	pe	Yang et al. (1992)
42182.41383	78706	0.00054	pe	Karetnikov & Medvedev (1977)	46179.22200	123912	-0.00144	pe	Yang et al. (1992)
42541.45935	82767	-0.00022	pe	Karetnikov & Medvedev (1977)	46211.13890	124273	-0.00173	pe	Yang et al. (1992)
42544.37635	82800	-0.00086	pe	Karetnikov & Medvedev (1977)	46211.22730	124274	-0.00174	pe	Yang et al. (1992)
42544.46585	82801	0.00023	pe	Karetnikov & Medvedev (1977)	56753.89238	243517	0.00014	CCD	Pena et al. (2017)
42548.44325	82846	-0.00097	pe	Mahdy & Szeidl (1980)	56753.98078	243518	0.00013	CCD	Pena et al. (2017)
42577.44425	83174	0.00048	pe	Karetnikov & Medvedev (1977)	57088.80307	247305	0.00137	CCD	Pena et al. (2017)
42871.50566	86500	-0.00063	pe	Mahdy & Szeidl (1980)	57114.79547	247599	0.00027	CCD	Pena et al. (2017)
42871.50746	86500	0.00117	pe	Karetnikov & Medvedev (1977)	57172.79276	248255	-0.00154	CCD	Pena et al. (2017)
42871.59386	86501	-0.00085	pe	Karetnikov & Medvedev (1977)	57175.79976	248289	-0.00059	CCD	Pena et al. (2017)
42872.47786	86511	-0.00098	pe	Karetnikov & Medvedev (1977)	57177.83176	248312	-0.00209	CCD	Pena et al. (2017)
42872.56636	86512	-0.00089	pe	Karetnikov & Medvedev (1977)	57459.87287	251502	0.00069	CCD	Pena et al. (2017)
42874.51126	86534	-0.00108	pe	Karetnikov & Medvedev (1977)	57460.84487	251513	0.00014	CCD	Pena et al. (2017)
43249.64837	90777	-0.00147	pe	Garrido et al. (1979)					